

University of Windsor

## Scholarship at UWindsor

---

Electronic Theses and Dissertations

Theses, Dissertations, and Major Papers

---

1991

### Unsupervised machine extraction of craniofacial landmarks for cephalometric evaluations.

John. Cardillo  
*University of Windsor*

Follow this and additional works at: <https://scholar.uwindsor.ca/etd>

---

#### Recommended Citation

Cardillo, John., "Unsupervised machine extraction of craniofacial landmarks for cephalometric evaluations." (1991). *Electronic Theses and Dissertations*. 4462.  
<https://scholar.uwindsor.ca/etd/4462>

This online database contains the full-text of PhD dissertations and Masters' theses of University of Windsor students from 1954 forward. These documents are made available for personal study and research purposes only, in accordance with the Canadian Copyright Act and the Creative Commons license—CC BY-NC-ND (Attribution, Non-Commercial, No Derivative Works). Under this license, works must always be attributed to the copyright holder (original author), cannot be used for any commercial purposes, and may not be altered. Any other use would require the permission of the copyright holder. Students may inquire about withdrawing their dissertation and/or thesis from this database. For additional inquiries, please contact the repository administrator via email ([scholarship@uwindsor.ca](mailto:scholarship@uwindsor.ca)) or by telephone at 519-253-3000ext. 3208.



National Library  
of Canada

Bibliothèque nationale  
du Canada

Canadian Theses Service    Service des thèses canadiennes

Ottawa, Canada  
K1A 0N4

## NOTICE

The quality of this microform is heavily dependent upon the quality of the original thesis submitted for microfilming. Every effort has been made to ensure the highest quality of reproduction possible.

If pages are missing, contact the university which granted the degree.

Some pages may have indistinct print especially if the original pages were typed with a poor typewriter ribbon or if the university sent us an inferior photocopy.

Reproduction in full or in part of this microform is governed by the Canadian Copyright Act, R.S.C. 1970, c. C-30, and subsequent amendments.

## AVIS

La qualité de cette microforme dépend grandement de la qualité de la thèse soumise au microfilmage. Nous avons tout fait pour assurer une qualité supérieure de reproduction.

S'il manque des pages, veuillez communiquer avec l'université qui a conféré le grade.

La qualité d'impression de certaines pages peut laisser à désirer, surtout si les pages originales ont été dactylographiées à l'aide d'un ruban usé ou si l'université nous a fait parvenir une photocopie de qualité inférieure.

La reproduction, même partielle, de cette microforme est soumise à la Loi canadienne sur le droit d'auteur, SRC 1970, c. C-30, et ses amendements subséquents.

# **Unsupervised Machine Extraction of Craniofacial Landmarks for Cephalometric Evaluations**

**by  
John Cardillo**

*A Dissertation*

*Submitted to the Faculty of Graduate Studies and Research  
through the Department of Electrical Engineering  
in Partial Fulfillment of the Requirements for the  
Degree of Doctor of Philosophy at the  
University of Windsor*

**Windsor, Ontario, Canada**

**1991**



National Library  
of Canada

Bibliothèque nationale  
du Canada

Canadian Theses Service    Service des thèses canadiennes

Ottawa, Canada  
K1A 0N4

**The author has granted an irrevocable non-exclusive licence allowing the National Library of Canada to reproduce, loan, distribute or sell copies of his/her thesis by any means and in any form or format, making this thesis available to interested persons.**

**The author retains ownership of the copyright in his/her thesis. Neither the thesis nor substantial extracts from it may be printed or otherwise reproduced without his/her permission.**

**L'auteur a accordé une licence irrévocable et non exclusive permettant à la Bibliothèque nationale du Canada de reproduire, prêter, distribuer ou vendre des copies de sa thèse de quelque manière et sous quelque forme que ce soit pour mettre des exemplaires de cette thèse à la disposition des personnes intéressées.**

**L'auteur conserve la propriété du droit d'auteur qui protège sa thèse. Ni la thèse ni des extraits substantiels de celle-ci ne doivent être imprimés ou autrement reproduits sans son autorisation.**

ISBN 0-315-69885-3

Canada

*11-8-11-91*

© *John Cardillo* 1991  
All Rights Reserved

# Abstract

A new automatic shape recognition algorithm has been developed to extract craniofacial landmarks from lateral skull x-rays (cephalograms). The locations of these landmarks are used by orthodontists in what is referred to as a cephalometric evaluation. The evaluation assists in the diagnosis of anomalies and in the monitoring of treatments. The algorithm is based on grey-scale mathematical morphology. A statistical approach with training was used to overcome subtle differences in skeletal topographies. Decomposition was used to desensitize the algorithm to size differences. Training was also used to minimize the search window sizes for improving speed and minimizing the detection of false targets. A system was trained to locate 20 landmarks. Test on 40 x-rays showed on average, 88% of the landmarks were located to within an acceptable accuracy of 2mm.

*To my loving wife  
Maria*

# Acknowledgments

It was a pleasure to work for Dr. M.A. Sid-Ahmed, my supervisor whom I admire and believe in. I thank him from my heart for all his guidance and support throughout my stay as a graduate student.

I also thank Dr. Bryan Williams for his kind help and for providing important access to cephalograms.

The Natural Sciences and Engineering Research Council of Canada is acknowledged for their scholarships and equipment grants which helped fund this research.

I also wish to thank the committee members, Dr. J.J. Soltis, Prof. P.H. Alexander, and Dr. G.W. Rankin for their valuable criticism and comments. I am grateful to Dr. K.P. Valavanis for coming from the University of Southwestern Louisiana to act as external examiner.

Finally, my most sincere appreciation is due to my family and friends, especially my mother and father, and Maria for their patience and faith in me.



# Table of Contents

<b>Abstract</b> .....	<b>iv</b>
<b>Acknowledgments</b> .....	<b>vi</b>
<b>List of Tables</b> .....	<b>x</b>
<b>List of Figures</b> .....	<b>xi</b>
<b>I. INTRODUCTION</b> .....	<b>1</b>
<i>A. Previous Work</i>	<i>1</i>
<i>B. Shape Recognition</i>	<i>2</i>
<i>C. Proposal</i>	<i>6</i>
<i>D. Dissertation Outline</i>	<i>7</i>
<b>II. CEPHALOMETRICS</b> .....	<b>8</b>
<i>A. History</i>	<i>8</i>
<i>B. The Cephalometric Radiograph</i>	<i>9</i>
<i>C. The Cephalometric Tracing</i>	<i>10</i>
<i>D. Landmarks</i>	<i>11</i>
<i>E. Reference Lines</i>	<i>15</i>
<i>F. Angular Measurements</i>	<i>18</i>
<i>G. Linear Measurements</i>	<i>20</i>
<i>H. Analysis</i>	<i>21</i>

<b>III. MATHEMATICAL MORPHOLOGY .....</b>	<b>23</b>
<i>A. Properties of Morphological Operators</i>	23
<i>B. Dilation</i>	25
<i>C. Erosion</i>	28
<i>D. Dilation Erosion Duality Theorem</i>	31
<i>E. Grey-Scale Morphology</i>	31
<b>IV. SHAPE RECOGNITION ALGORITHM .....</b>	<b>36</b>
<i>A. The Generic Shape Recognition Algorithm</i>	37
1. The Grey-level Shape Recognition Algorithm	38
2. Decomposition	42
3. Summary	48
4. Locating the Minimum	48
5. Example	50
<i>B. Training</i>	55
1. Updating the Structuring Element	56
2. Updating the Location Distribution	58
3. Example	59
<b>V. SEARCH WINDOWS .....</b>	<b>62</b>
<i>A. Estimation of Translational, Rotational and Size Differences</i>	64
<i>B. Window Training</i>	66
<i>C. Transforming the Structuring Element Positions</i>	68
<b>VI. EXPERIMENTAL RESULTS .....</b>	<b>70</b>
<i>A. Experiment 1 — Locating Before Training</i>	74

1. Purpose	74
2. Procedure	74
3. Observations	74
4. Discussion	76
<i>B. Experiment 2 — Locating after training</i>	81
1. Purpose	81
2. Procedure	81
3. Observations	81
4. Discussion	81
<b>VII. RECOMMENDATIONS FOR FUTURE WORK</b>	<b>.86</b>
<i>A. Multiple Models per Landmark</i>	86
<i>B. Variable Sized Structuring Elements</i>	87
<i>C. Variable Resolution Structuring Elements</i>	89
<i>D. Search Window Shapes</i>	89
<b>VIII. CONCLUSIONS</b> .....	<b>.90</b>
<i>A. Contribution</i>	90
<i>B. Summary of Results</i>	90
<b>IX. REFERENCES</b> .....	<b>.92</b>
<b>Vita Auctoris</b> .....	<b>.96</b>

# List of Tables

2.1	REFERENCE POINTS .....	12
2.2	REFERENCE LINES .....	16
2.3	ANGULAR MEASUREMENTS .....	18
2.4	LINEAR MEASUREMENTS .....	20
3.1	PROPERTIES OF DILATION .....	27
3.2	PROPERTIES OF EROSION .....	30
6.1	DEFINED TEST LANDMARKS .....	72
6.2	LOCATION ERRORS FOR EXPERIMENT #1 .....	75
6.3	LOCATION ERRORS FOR EXPERIMENT #2 .....	82
6.4	STATISTICAL SUMMARY OF LOCATION ERRORS IN EXPERIMENT #2 .....	85

# List of Figures

1.1	An example of different images which produce the same cross-correlation. ....	4
2.1	A typical cephalogram or lateral skull x-ray. ....	9
2.2	A cephalometric tracing of bony and soft tissue outlines. ....	10
2.3	Commonly used reference landmarks as defined on the cephalogram. ....	14
2.4	Commonly used reference landmarks as defined on the cephalometric tracing. ....	15
2.5	Commonly used reference lines. ....	17
2.6	Commonly used angular measurements. ....	19
2.7	Commonly used linear measurements. ....	21
3.1	Dilation of a binary image. ....	26
3.2	Erosion of a binary image. ....	29
3.3	Illustration of the dilation erosion duality theorem. ....	32
3.4	The cross-section of a grey-level surface and the umbra of the surface. ....	32
3.5	Cross-sectional view of grey-level dilation. ....	35

3.6	Cross-sectional view of grey-level erosion. ....	35
4.1	The erosion of a binary image by a small disk. ....	36
4.2	The generic shape recognition algorithm applied to a binary image. ....	37
4.3	The generic shape recognition algorithm applied to a cross section of a grey-level image. ....	39
4.4	The generic shape recognition algorithm applied to a corrupted image. ....	41
4.5	An example of a shape which for varying sizes will (a) not pose a problem to the shape recognition algorithm and, (b) will be difficult to find with the shape recognition algorithm. ....	43
4.6	A tracing of the landmark sella (a) decomposed into 3 structuring elements, and (b) the locations of these structuring elements on a larger version of the landmark. ....	45
4.7	A tracing of the landmark sella. Search results overlap in (a) and (b) when the point origins are replaced by probability distributions. ....	45
4.8	Shape recognition applied to a grey-level landmark consisting of two structuring elements. Dredging is used to shape the minimums such that when combined they overlap. ....	46
4.9	Problems with locating the minimum in a digital image. ....	49
4.10	A digital x-ray image of the landmark sella and its defining structuring elements. ....	51

4.11	An x-ray to be processed and the search window for locating sella. ....	51
4.12	The shape recognition error function when searching with the first structuring element. ....	52
4.13	The shape recognition error function when searching with the second structuring element. ....	52
4.14	The combined results from the first and second structuring elements. ....	53
4.15	The shape recognition error function when searching with the third structuring element. ....	53
4.16	The combined search results from all three structuring elements. .	54
4.17	The position of sella located at the minimum in the combined error function. ....	54
4.18	Training the landmark sella by (a) assigned search windows for finding the structuring elements, (b) locating the positions of the structuring elements, (c) extracting training data from the located positions, and (d) using the difference in the located positions from the defined positions to update the location distribution. ....	56
4.19	Structuring element training procedure. ....	57
4.19	Training the location distribution by averaging (a) spikes, and (b) Gaussian distributions. ....	59

4.20	The located and verified position of sella on an x-ray to be used for training. ....	60
4.21	The search results from the automatic training algorithm as it finds the first structuring element. ....	60
4.22	The search results from the automatic training algorithm as it finds the second structuring element. ....	61
4.23	The search results from the automatic training algorithm as it finds the third structuring element. ....	61
5.1	Transforming defined search windows onto the target x-ray. ....	63
6.1	The cephalometrics work station. ....	71
6.2	The test landmarks used in the experiments. ....	73
6.3	Plot of number of landmarks located within an error of (i) 2mm, (ii) 5mm, and (iii) were within the search window. ....	76
6.4	Plot of number of landmarks located to within an error of (i) 2mm, (ii) 5mm, and (iii) further than 5mm, as a % of those points which were within the search window. ....	77
6.5	Summarized results per landmark. Number of times located to within an error of (i) 2mm, (ii) 5mm, and (iii) further than 5mm, as a % of those which were within the search window. ...	79
6.6	Plot of the time required to locate 20 landmarks over 40 x-rays. .	80
6.7	Summarized results per landmark. Number of times located to within an error of (i) 2mm, (ii) 5mm, and (iii) further than 5mm, as a % of those which were within the search window. ...	83



7.1 An example of the possible unwanted interference caused by the lips on the structuring element defining the tip of the incisors. . . 88

# I. INTRODUCTION

There are some 20 - 30 anatomical landmarks visible on lateral skull x-rays that are commonly used by orthodontists in what is called a cephalometric evaluation [1]. The locations of these points form the basis of a series of angular and linear measurements that make up the evaluation. At present these landmarks are located by hand or digitized using a graphics tablet. The task is usually carried out in two steps. First, a simplified tracing is made of the bony and soft tissue outlines visible on the x-ray. Then, the landmark locations are extracted from corners, intersections and other extremum points on these lines. This tedious process is subject to human error and needs to be repeated for each patient. Therefore, the motivation exists to automate this repetitive and time consuming process.

## *A. Previous Work*

Previous attempts to automate the landmarking of cephalograms followed a strategy similar to that used by orthodontists. These approaches employed a combination of image processing techniques to extract the important edges first. Landmark locations are then found on the edges using a geometrical description of the landmark. For example, the tip of the nose is found on the most anterior point of the outline of the nose.

Some of the earliest research was by Lévy-Mandel *et al.* [2] who used a knowledge-based line extraction technique. They begin by first pre-processing the digital x-ray image using histogram equalization and median filtering to enhance contrast and remove some noise. The

Mero-Vassy operator [3] was then used to enhance edges. The relevant edges are then extracted using a knowledge-based line tracker. Lines are tracked in a pre-determined order following a set of knowledge-based rules toward set goals. The landmarks are then located on these lines according to their geometric definitions. Unfortunately, the algorithm cannot be used to locate landmarks which do not lie on edges. The algorithm also relies on good quality x-rays, something which cannot be guaranteed in practice.

Nugent *et al.* [4], [5] also proposed a method using a knowledge-based line extractor. In addition, they used a resolution pyramid to improve processing time. A  $512 \times 480$  digital x-ray image is first operated on at a much reduced resolution of  $64 \times 60$ . Once the landmarks are found the resolution is increased by factors of two and the locations are fine tuned. However, the line tracking algorithm is somewhat ad-hoc, as various edges are traced and landmarks located according to the authors' geometric description of them.

Contreras-Vidal and Garza-Garza [6], Jackson *et al.* [7], Cohen and Linney [8], and Cohen *et al.* [9] also approached the problem with some form of knowledge-based edge tracking.

The main problem with these techniques is that they require consistent good quality x-rays. If an x-ray contains extra lines, which is often the case because of the symmetric features on either side of the face, or if the x-ray is poorly exposed resulting in fragmented lines, the critical lines defining the landmarks may not be tracked properly.

### ***B. Shape Recognition***

Instead of trying to duplicate the orthodontist by extracting edges first, why not attempt to locate the landmarks directly? After all, it is the location of the landmarks which is critical to the measurements. If

necessary, the tracing could be obtained later by fitting a standard set of curves to the located landmarks. The line tracing will not be as precise, but most of the emphasis is placed on the landmark locations as it should be. The problem is then one of shape recognition, also known as image matching or object recognition.

A desirable feature of the cephalometric shape recognition algorithm is to allow the orthodontist to define a set of landmarks. Training could be used to teach the algorithm the shapes and locations of the landmarks as judged by the orthodontist. This is desirable because orthodontists do not always share the same views and preferences when it comes to a selection of landmarks. Also, one may wish to experiment with new landmark definitions. Personalizing is possible if a general shape recognition algorithm is developed.

Most image matching schemes are based on either minimizing the mean squared error or maximizing the image correlation [10]-[13]. Let the signal  $f$  represent an image in which the image  $g$  of size  $W$  is being sought. Let  $k$  represent a shifting vector which translates the image  $g$  over the image  $f$ . Then, the root square error function to be minimized is

$$E(k) = \sqrt{\sum_{n \in W} [f(n+k) - g(n)]^2}. \quad (1.1)$$

A more popular error function is the sum of absolute differences computed as

$$E(k) = \sum_{n \in W} |f(n+k) - g(n)|. \quad (1.2)$$

This function is more popular because it requires only addition and sign changes, while the mean squared error uses multiplication.

Matching using classical linear cross-correlation involves searching for the maximum using

$$L_{fg}(k) = \sum_{n \in W} f(n+k)g(n). \quad (1.3)$$

where  $L_{fg}(k)$  is the cross-correlation of  $f(x)$  with  $g(x)$ . Cross-correlation methods work well for either signals that maintain a zero average such as communication and radar signals or in cases such as images where a zero average or  $\sum_{n \in W} g(n) = 0$  has been enforced. Although a maximum produced

by cross-correlation satisfies necessary conditions for a match it is not sufficient. It is easy to produce an example where the maximum does not represent a match. Figure. 1.1 shows a  $3 \times 3$  template and 3 different  $3 \times 3$  images which will produce the same cross-correlation.

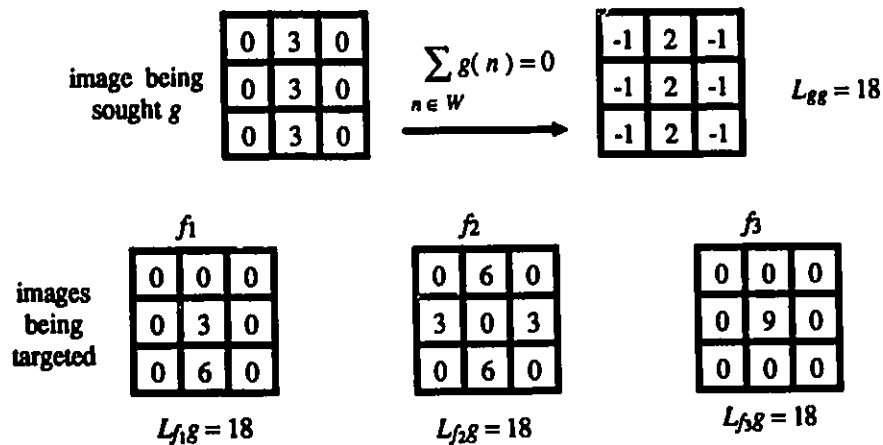


Fig. 1.1. An example of different images which produce the same cross-correlation.

Classification techniques based on feature extraction such as nearest neighbor [14], Bayesian learning systems [15], and neural networks [16] also may be used to locate shapes but they are not intended to work in a cluttered scene. They are better suited for identifying isolated objects on a uniform background such as printed characters. In this problem the landmarks are not usually available as bound objects. They are shapes which are embedded throughout a cluttered image.

Shape recognition techniques based on mathematical morphology, are ideally suited for the analysis of bound and unbound shapes. Crimmins and Brown [17] showed how mathematical morphology could be used to locate shapes by matching both the image and its complement. In binary images, if the white pixels constitute the image then all the black pixels are its complement. When searching for a donut shaped object, for example, verifying the presence of a ring is necessary but it would not be sufficient. It may also be necessary to verify the presence of a hole. Thus, this shape recognition technique provides both necessary and sufficient conditions to locate objects. In contrast, such schemes as cross-correlation provide only necessary conditions for shape recognition.

Grey-level images are treated as three dimensional surfaces where the grey-level is the z-coordinate. The volumetric region beneath the surface is considered the image while the region above the surface is the complement of the image. Matching grey-level images is then a matter of fitting a template to an image and its complement.

Shapiro *et al.* [18] and, Shih and Mitchell [19] describe methods using mathematical morphology to extract primitives or parts of an object. Objects are then recognized by analyzing the relational positions of those primitives. However, this technique is better suited for recognizing isolated

objects where the memberships of the various primitives are easily determined.

Maragos [20] presents a morphological equivalent to the minimization of the mean squared error or the maximization of the cross-correlation. He defines the morphological cross-correlation  $M_{fg}(k)$  as the sum of minima

$$M_{fg}(k) = \sum_{n \in W} \min[f(n+k), g(n)]. \quad (1.4)$$

Maximizing this function provides a good matching criterion provided that the factor  $\sum_{n \in W} f(n+k)$  does not fluctuate drastically through the image. This factor represents the DC level in the image near and around  $k$ . It provides no local shape information but will affect  $M_{fg}$ . If this factor varies globally, the maximizing of  $M_{fg}$  becomes an unreliable matching criterion.

### ***C. Proposal***

In this study, grey-scale morphological operators are used to devise a new shape recognition algorithm to locate landmarks on  $512 \times 480$  digital x-ray images. The algorithm is an extension of that proposed by Crimmins and Brown [17]. The scheme is tailored to the problem at hand but kept general so that one algorithm may be applied to locate any defined landmark. Thus, with the help of a novel training scheme a system based on this technique may be easily personalized to locate any set of landmarks according to the orthodontist's preferences. Also, by incorporating some probability theory, the approach may circumvent some of the rigid properties of the morphological operations, making this

technique less susceptible to noise and more accommodating to subtle variations in skeletal topographies.

To minimize the processing time, a technique is developed to decrease the amount of image which must be searched to find each landmark. The positions of located landmarks may be used to predict or at least narrow down the possible positions of subsequent points. If the system is trained to remember the possible relative positions of the landmarks, then as points are being located this information may be used to optimize the search for subsequent points.

The developed algorithms are tested on 40 randomly selected x-rays obtained from male and female patients ranging from 9 to 39 years of age. To simulate realistic operating conditions, the x-rays are not screened. These tests are performed to assess both the recognition and the progress during training.

#### ***D. Dissertation Outline***

The thesis begins with introductory chapters on cephalometrics and mathematical morphology. These chapters serve to define the problem and to provide a mathematical basis for the solution. Shape recognition using mathematical morphology is discussed in chapter 4. The chapter describes a new technique using a statistical approach together with decomposition and training to accommodate subtle differences in skeletal topographies. Chapter 5 examines search windows and presents a new technique for minimizing their sizes. In the remaining chapters the shape recognition algorithm is evaluated through a set of experiments. Recommendations for improving the algorithm and conclusions are drawn from the experimental results.



## II. CEPHALOMETRICS

Cephalometry is the scientific measurement of the dimensions of the head. Cephalometrics is a tool that provides a quantitative assessment or description of craniofacial morphology. The measurements may be compared with norms, ideals or previous measurements of one's self. These comparisons help in the diagnosis of anomalies, monitoring of treatments, and growth predictions.

### *A. History*

Assessing craniofacial dimensions dates back centuries ago, though the motivation was artistic then. During the Renaissance, for example, Leonardo DaVinci, studied the proportions of the head, and body in an attempt to quantify beauty. Later, anthropologists began using skull measurements to compare and categorize ancestral human skulls. Methods of measurements were developed that proved to be of value to orthodontics. During the 1930's, the use of x-ray pictures of the skull was introduced to orthodontics and cephalometric radiography was born. Since then a variety of analyses have been developed based on the standard lateral radiograph of the skull. These analyses are composed of a series of angular and linear measurements designed to provide an assessment of the facial skeleton, the teeth, and soft tissue profile. The reference points or landmarks used to generate these measurements are critical. The effectiveness of an evaluation depends on an accurate definition and localization of the landmarks.

### ***B. The Cephalometric Radiograph***

Cephalometric radiographs or cephalograms are produced using an x-ray source, film holder and a cephalostat or head holder. The x-ray tube source is placed 2-4 meters from the subject and the film holder is placed on the opposite side as near to the subject as possible. This minimizes distortions or enlargement when reproducing the projection of the skull.

For the standard lateral projection shown in Fig. 2.1 The subject is placed with the left side towards the film. European standards place the right side towards the film. The centre of the x-ray beam coincides with the ear rods of the cephalostat.

The quality of the radiograph may be marred by improper exposures. Soft tissues are more easily penetrated by the x-rays than are



**Fig. 2.1.** A typical cephalogram or lateral skull x-ray.

the bony masses. Consequently, problems arise when trying to strike a balance where both tissue types are adequately imaged. A barrier is often placed near the front of the face to reduce the intensity of the x-rays penetrating the soft tissues of the face. When improperly placed this barrier sometimes interferes with imaging of the facial skeleton.

### ***C. The Cephalometric Tracing***

The cephalogram is rarely used directly in the analysis. Instead, a tracing similar to the one shown in Fig. 2.2 is first made of the important bony and soft tissue outlines visible on the cephalogram. Tracings from subsequent x-rays are superimposed and compared to monitor treatments or assess growth. Superimposing x-rays would be nearly impossible to analyze. Care must be taken to trace accurately through the important landmarks whose positions are critical to the measurements.



**Fig. 2.2.** A cephalometric tracing of bony and soft tissue outlines.

#### ***D. Landmarks***

The shapes of structures within the skull depend on several factors such as age, sex, race, etc. The selection of a standard set of landmarks, therefore, is not straightforward. Overlapping anatomical features also present a problem. The shapes of the landmarks may differ in two x-rays taken from the same patient. A slight shift in the orientation of the skull when x-rays are taken may cause a shift in overlapping features. It is through experience that an observer is able to recognize a landmark and its possible variations.

There are several kinds of landmarks used in cephalometric evaluations and they are described as follows:

- (1) ***Anatomic Points*** – Anatomic points are small regions located on the solid skull. Examples include; sella (S), nasion (Na) and the anterior nasal spine (ANS).
- (2) ***Implants*** – Implants are artificial markers which show up on the radiograph. They are more clearly visible and easier to locate than anatomic landmarks but, their positions from subject to subject are not consistent. Studies based on implants are thus difficult and less accurate.
- (3) ***Extremal Points*** – Extremal points are characterized as falling on extrema of curvatures. Examples include; A point (A), B point (B), and gnathion (Gn).
- (4) ***Intersection of Edges*** – These intersections are points which do not actually exist on the skull but are the result of intersecting outlines visible on the x-ray projection. Examples include; articulare (Ar), and pteryomaxillary fissure (PTM).
- (5) ***Intersection of Lines*** – Line intersects are constructed points based on the intersection of projected lines. For example, the anterior point for determining the length of mandible (APmax) is formed by dropping a perpendicular from pogonion (Pog) to the mandibular plane.

Of the various types of landmarks the first four must be extracted from the cephalogram.

Table 2.1 lists some more commonly used landmarks according to [1] and [21]. The actual selection of landmarks used by each orthodontist varies with personal preference and experience. Figure 2.3 and 2.4 illustrate the position and shapes of these landmarks as viewed on a typical cephalogram and tracing.

**TABLE 2.1.**  
**REFERENCE POINTS**

No.	Abbreviation	Definition
1	N	<i>Nasion.</i> The most anterior point of the nasofrontal suture in the median plane. The skin nasion ( $N^1$ ) is located at the point of maximum convexity between nose and forehead.
2	S	<i>Sella.</i> The sella point is defined as the midpoint of the hypophysial fossa. It is a constructed radiological point in the median plane.
3	Se	<i>Midpoint of the entrance to the sella.</i> This point represents the midpoint of the line connecting the posterior clinoid process and the anterior opening of the turcica.
4	Sn	<i>Subnasale.</i> A skin point where the nasal septum merges mesially with the integument of the upper lip.
5	A	<i>Point A, subspinale.</i> The deepest midline point in the curved bony outline from the base to the alveolar process of the maxilla.
6	APMax	<i>The anterior landmark for determining the length of the maxilla.</i> It is constructed by dropping a perpendicular from point A to the palatal plane.
7	Pr	<i>Prosthion.</i> Alveolar rim of the maxilla; the lowest, most anterior point on the alveolar portion of the premaxilla, between the upper central incisors.
8	Is or Is $\perp$	<i>Incisor superioris.</i> Tip of the crown of the most anterior maxillary central incisor.
9	Ap $\perp$	<i>Apicale I.</i> Root apex of the most anterior maxillary central incisor.

No.	Abbreviation	Definition
10	Ii or Is $\bar{1}$	<i>Incisor inferious.</i> Tip of the crown of the most anterior mandibular central incisor.
11	Ap $\bar{1}$	<i>Apicale <math>\bar{1}</math>.</i> Root apex of the most anterior mandibular central incisor.
12	Id	<i>Infradentale.</i> Alveolar rim of the mandible; the highest, most anterior point on the alveolar process, in the median plane, between the mandibular central incisors.
13	B	<i>Point B, supramentale.</i> Most anterior part of the mandibular base. It is the most posterior point in the outer contour of the mandiblar alveolar process, in the median plane.
14	Pog	<i>Pogonion.</i> Most anterior point of the bony chin, in the median plane.
15	Gn	<i>Gnathion.</i> It is located between the most anterior and the most inferior point of the bony chin.
16	Go	<i>Gonion.</i> A constructed point, the intersection of the lines tangent to the posterior margin of the ascending ramus and the mandibular base.
17	Me	<i>Menton.</i> It is the lowest point of the mandible.
18	APMan	<i>The anterior landmark for determining the length of the mandible.</i> It is defined as the perpendicular dropped from Pog to the mandibular plane.
19	ar	<i>Articulare.</i> The intersection of the posterior margin of the ascending ramus and the outer margin of the cranial base.
20	Cd	<i>Condylion.</i> Most superior point on the head of the condyle.
21	Or	<i>Orbitale.</i> Lowermost point of the orbit in the radiograph.
22	Soft Pog	<i>Soft tissue Pogonion.</i> Most anterior point of the skin of the chin in the median plane.
23	Nose	<i>Tip of the Nose.</i> The most anterior point of the skin of the nose in the median plane.
24	ANS	<i>Anterior nasal spine.</i> The tip of the bony anterior nasal spine in the median plane.
25	PNS	<i>Posterior nasal spine.</i> A constructed radiological point marking the intersection of a continuation of the anterior wall of the pterygopalatine fossa and the floor of the nose. It marks the dorsal limit of the maxilla.

No.	Abbreviation	Definition
26	S'	<i>Landmark for assessing the length of the maxillary base, in the posterior section.</i> It is defined as a perpendicular dropped from point S to a line extending the palatal plane.
27	APOcc	<i>Anterior point for the occlusal plane.</i> A constructed point, the midpoint in the incisor overbite in occlusion.
28	PPOcc	<i>Posterior point for the occlusal plane.</i> The most distal point of contact between the most posterior molars in occlusion.
29	Ba	<i>Basion.</i> Lowest point on the anterior margin of the foramen magnum in the median plane
30	Ptm	<i>Pterygomaxillary fissure.</i> The contour of the fissure projected onto the palatal plane.



Fig. 2.3. Commonly used reference landmarks as defined on the cephalogram.

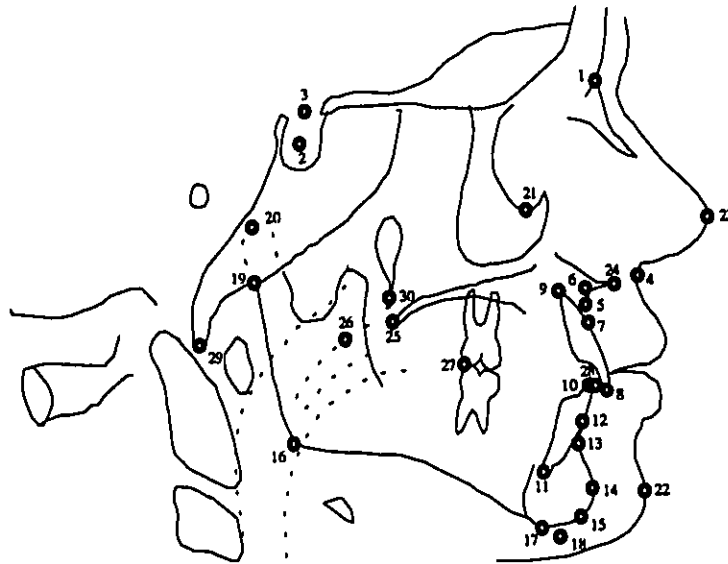


Fig. 2.4. Commonly used reference landmarks as defined on the cephalometric tracing.

### ***E. Reference Lines***

The locations of the landmarks described above form the basis for the construction of a series of lines and planes. The lengths of some lines provide linear measurements while the angles between others provide angular measurements. There are three basic types of lines which can be constructed.

- (1) ***Lines joining two landmarks*** – The simplest reference lines are defined using the locations of two located landmarks. An example is the palatal plane formed by joining (ANS) and (PNS).
- (2) ***Lines passing through a landmark and parallel to another defined line*** – These lines are used to project linear measurements to a defined reference line.



(3) *Lines passing through a landmark and perpendicular to another line –*

These lines are used to calculate distances from points to lines.

Table 2.2 lists some more frequently used reference lines according to [1]. These are illustrated in Figure 2.5.

**TABLE 2.2.  
REFERENCE LINES**

No.	Line	Definition
1	S-N	Sella-nasion. Anteroposterior extent of anterior cranial base.
2	S-Ar	Lateral extent of cranial base.
3	ar-Go	Length of ramus.
4	Me-Go	Extent of mandibular base.
5	N-A	Nasion - point A.
6	N-B	Nasion - point B
7	N-Pr	Nasion - prosthion.
8	N-Id	Nasion - infradentale.
9	N-Pog	Nasion - pogonion.
10	N-Go	Nasion - gonion line, for analysis of the gonial angle.
11	Pal	Palatal plane (ANS-PNS).
12	Occ	Occlusal plane (APOcc-PPOcc).
13	S-Gn	Y-axis.
14	S-Go	Posterior facial height.
15	1-SN	Long axis of upper incisor to SN.
16	1-Pal	Long axis of upper incisor to Pal.
17	$\bar{1}$ -MP	Long axis of lower incisor to mandibular plane.
18	ManBase	Extent of mandibular base (Go-Gn).

No.	Line	Definition
19	MaxBase	Extent of maxillary base (APMax-PNS).
20	R.asc.	Cd-Go length of ramus.
21	S-S'	Perpendicular from point S (starting from the SN line) to point S'.
22	Pn line	Perpendicular to SeN, from the soft tissue nasion N <sup>1</sup> as far as Pal.
23	H line	Modified Frankfurt horizontal; parallel to the SeN line which bisects the Pn line from N to Pal (Pn/2 - FH/R.asc.).
24	EL	Aesthetic line. Tip of nose - soft tissue pogonion.

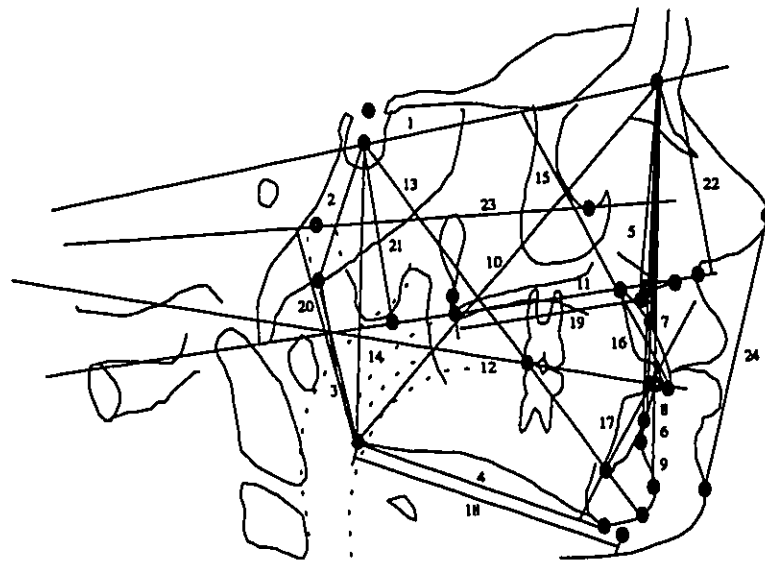


Fig. 2.5. Commonly used reference lines.

### ***F. Angular Measurements***

These reference lines are used to make angular measurements of skull geometries. Table 2.3 lists some routine angular measurements taken according to [1]. They are described with statistical norms and variations. Figure. 2.6 illustrates these angles on the cephalometric tracing.

**TABLE 2.3.  
ANGULAR MEASUREMENTS**

<b>No.</b>	<b>Points of the angle</b>	<b>Definition</b>	<b>Mean value</b>
1	N-S-Ar	Saddle angle	$123^{\circ} \pm 5^{\circ}$
2	S-Ar-Go	Articular angle	$143^{\circ} \pm 6^{\circ}$
3	Ar-Go-Me	Gonial angle	$128^{\circ} \pm 7^{\circ}$
4	Sum	Sum of sella, articular and gonial angles	$394^{\circ}$
5	Ar-Go-N	Go <sub>1</sub> , upper gonial angle	$52^{\circ} - 55^{\circ}$
6	N-Go-Me	Go <sub>2</sub> , lower gonial angle	$70^{\circ} - 75^{\circ}$
7	SNA	Anteroposterior position of maxilla	$81^{\circ}$
8	SNB	Anteroposterior position of mandible	$79^{\circ}$
9	ANB	Difference between SNA and SNB	$2^{\circ}$
10	S-N-Pr	Anteroposterior position of alveolar part of premaxilla	$84^{\circ}$
11	S-N-Id	Anteroposterior position of alveolar part of mandible	$81^{\circ}$
12	Pal-MP	Angle between palatal and mandibular plane	$25^{\circ}$
13	Pal-Occ	Upper occlusal plane angle	$11^{\circ}$
14	MP-Occ	Lower occlusal plane angle	$14^{\circ}$
15	SN-MP	Angle between SN and mandibular plane	$32^{\circ}$

No.	Points of the angle	Definition	Mean value
16	Pn-Pal	Angle of inclination	85°
17	N-S-Gn	(Y-axis) Angle between SN line and S-Gn line, anteriorly	66°
18	I-SN	Angle between upper incisor axis and SN line posteriorly	102°
19	I-Pal	Angle between upper incisor axis and palatal plane, anteriorly	70° ± 5°
20	$\bar{I}$ -MP	Angle between lower incisor axis and mandibular plane, posteriorly	90° ± 3°
21	ii angle	Interincisal angle between upper and lower central incisor axes, posteriorly	135°

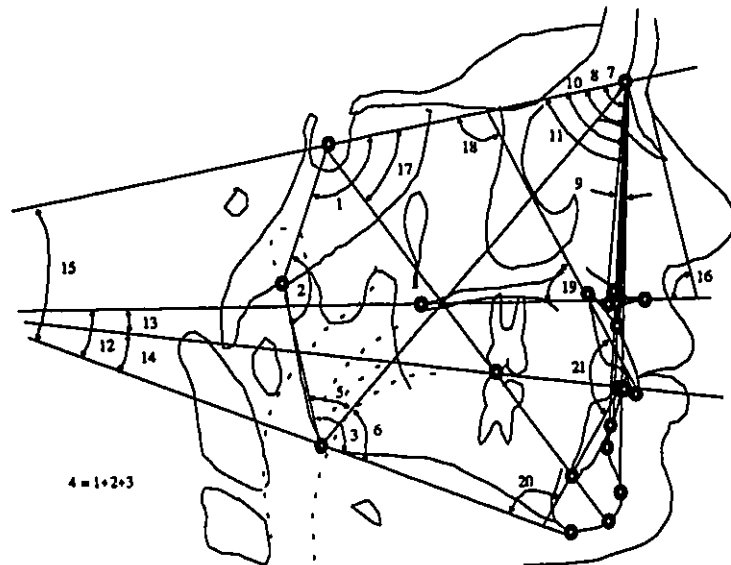


Fig. 2.6. Commonly used angular measurements.

### G. Linear Measurements

There are two basic types of linear measurements.

(1) **Point to point** – Point to point distances are simply calculated between located points. An example is the anteroposterior extent of anterior cranial base (S-N) measured from (S) to (Na).

(2) **Point to line** – Point to line distances are perpendicular distances from a point to a line. An example is the distance from incisal edge 1 to N-Pog line.

Table 2.4 lists some of the commonly used linear measurements. These are illustrated in Fig. 2.7.

**TABLE 2.4.**  
**LINEAR MEASUREMENTS**

No.	Distance	Definition	Mean value
1	S-N	(SeN) Anteroposterior extent of anterior cranial base	71mm
2	S-Ar	Extent of lateral cranial base	32-35 mm
3	S-Go	Posterior facial height	
4	N-Me	Anterior facial height	
5	MaxBase	Extent of maxillary base, correlated with Se-N	
6	ManBase	Extent of mandibular base, correlated with Se-N	
7	R.asc.	Extent of ascending ramus, correlated with SeN	
8	S'-F.Ptp.	Distance from S' to projection of the anterior wall of the pterygopalatal fossa onto the palatal plane, expression for anteroposterior displacement of the maxillary base	
9	S-S'	Expression for deflections of the maxillary base	42-57mm
10	1-N-Pog	Distance from incisal edge of 1 to N-Pog line	
11	$\bar{1}$ -N-Pog	Distance from incisal edge of $\bar{1}$ to N-Pog line	

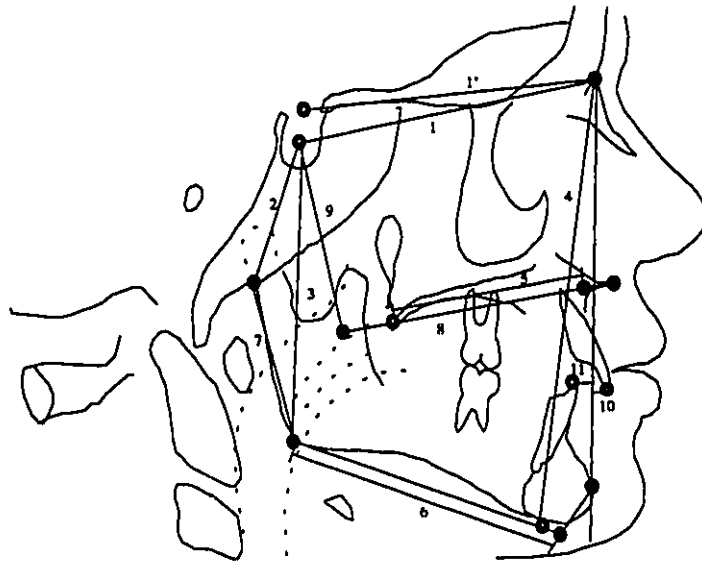


Fig. 2.7. Commonly used linear measurements.

### ***H. Analysis***

The angular and linear measurements described are not usually analyzed independently. Rather, measurements are compared, correlated, normalized and combined to produce a variety of analyses. These analyses are divided into two basic groups consisting of several stages of analysis as follows:

- (1) **Dento-Skeletal Analysis**
  - (a) **Analysis of facial skeleton**
  - (b) **Analysis of mandibular and maxillary base**
  - (c) **Dento alveolar analysis**

**(2) Soft-Tissue Analysis**

- (a) Profile analysis**
- (b) Lip analysis**
- (c) Tongue analysis**

The generation of these analyses is a routine and tedious task. Seldom does a subject require special consideration beyond the normal measurements. The generation of these measurements is thus ideally suited for automation. Orthodontists would be freed from the rigor and could concentrate their efforts on the medical interpretation of these measurements.

### III. MATHEMATICAL MORPHOLOGY

Mathematical morphology is an image processing approach ideally suited for the analysis of structure and form. Its initiation by Matheron in 1964 together with work by Serra led to the formation of the Centre de Morphologie Mathematique at the Paris School of Mines. Matheron published a book on the mathematical basis of morphology entitled "Random Sets and Integral Geometry" [22]. Later, Serra's book provided theory coupled with application examples on image analysis [23]. Since then, mathematical morphology has been steadily gaining popularity in the image processing community. Papers by Heijmans and Ronse [24], and Serra [25] provide an in-depth overview of the theory. Papers by Meyer [26], Haralick *et al.* [27], and Sternberg [28] demonstrate some practical uses of mathematical morphology to image analysis.

This chapter is an introduction to mathematical morphology intended to provide the reader with some background of the mathematics used in the shape recognition algorithm to be developed in the next chapter. It describes the basic morphological operations of dilation and erosion. The language is set theory. Sets in Euclidean 2D-space represent binary images while sets in Euclidean 3D-space are used to represent grey-level images. In general, the operations are defined in Euclidean N-space or  $E^N$ .

#### ***A. Properties of Morphological Operators***

The basic properties commonly used to describe morphological transforms are defined as follows: ( $\Psi$  represents the generic symbol of a morphological transform)



1. **Increasing** –  $\Psi$  is said to be increasing if, when a set  $X$  is included in  $Y$ , the transform  $\Psi(X)$  is also included in the transform  $\Psi(Y)$ .

$$X \subset Y \Rightarrow \Psi(X) \subset \Psi(Y) .$$

2. **Extensivity or Anti-extensivity** –  $\Psi$  is extensive if the transform of a set includes the set.

$$\Psi(X) \supset X .$$

$\Psi$  is anti-extensive if the set includes the transform of itself.

$$\Psi(X) \subset X .$$

3. **Idempotence** –  $\Psi$  is idempotent when applying the operator more than once has no effect.

$$\Psi[\Psi(X)] = \Psi(X) .$$

4. **Homotopy** –  $\Psi$  is homotopic when it preserves the particle-in-hole, hole-in-particle relationship or the homotopic tree of a bounded set. The homotopic tree of a set has a trunk corresponding to the background and branches corresponding to the connected components. In other words, if boundaries between objects are lost due to the transform then the transform is not homotopic.
5. **Compatibility with Translation** – Translating a set  $X$  by a vector  $h$  is denoted  $X_h$  and is defined by

$$X_h = \{x + h \mid x \in X\}$$

$\Psi$  is invariant under translation if

$$\Psi(X_h) = [\Psi(X)]_h$$

If  $\Psi$  depends on the origin, denoted  $\Psi^o$ , then this condition no longer holds. With the exception of a translation, it is the same to shift  $X$  by  $h$  as it is to shift  $\Psi$  by  $-h$ . Therefore, a more general criterion known as compatibility under translation is

$$\Psi^o ( X_h ) = [ \Psi^{-h} ( X ) ]_{+h}$$

6. **Compatibility with Magnification** – Magnifying a set  $X$  by a scalar  $\lambda$  is denoted  $\lambda X$  and is defined by

$$\lambda X = \{ x \lambda \mid x \in X \}.$$

$\Psi$  is invariant under magnification if

$$\Psi(\lambda X) = \lambda \Psi(X).$$

However, most transformations depend on some scale factor. A family of transformations  $\Psi_\lambda$  is said to be compatible under change of scale if

$$\Psi_\lambda ( X ) = \lambda \Psi \left( \frac{X}{\lambda} \right).$$

Although the functions within this family operate at different scales, they are performing essentially the same task and are therefore compatible.

7. **Associativity** –  $\Psi$  is associative if

$$\Psi[ \Psi( X, Y ), Z ] = \Psi[ X, \Psi( Y, Z ) ].$$

8. **Commutivity** –  $\Psi$  is commutative if

$$\Psi( X, Y ) = \Psi( Y, X ).$$

9. **Distributivity** –  $\Psi$  distributes over some operator  $\xi$  if

$$\Psi[ X, \xi( Y, Z ) ] = \xi[ \Psi( X, Y ), \Psi( X, Z ) ].$$

## **B. Dilation**

Let  $A$  and  $B$  be sets in  $E^N$ . The  $N$ -dimensional vectors  $a = (a_1, a_2, \dots, a_N)$  and  $b = (b_1, b_2, \dots, b_N)$  represent elements in  $A$  and  $B$  respectively. The dilation of  $A$  by  $B$ , denoted  $A \oplus B$ , is defined as all the possible vector sums of elements, one from  $A$  with one from  $B$  written

$$A \oplus B = \{ a + b \mid a \in A, b \in B \}. \quad (3.1)$$

Since vector addition is a translation, dilation may also be expressed as the union of translations of  $A$  by the elements of  $B$ . The commutivity of addition also permits dilation to be defined as the union of translations of  $B$  by the elements of  $A$ . Symbolically,

$$A \oplus B = \bigcup_{b \in B} A_b = \bigcup_{a \in A} B_a . \quad (3.2)$$

Dilation is analogous to planting at the points in  $A$ , seeds from which the set  $B$  is grown. In practice the operand  $A$  is considered the image while the operand  $B$  is referred to as the structuring element. Figure 3.1 illustrates the dilation of a binary image. In this example the set space is the two dimensional grid. The image  $A$  is the set of all the black pixels on the white grid.

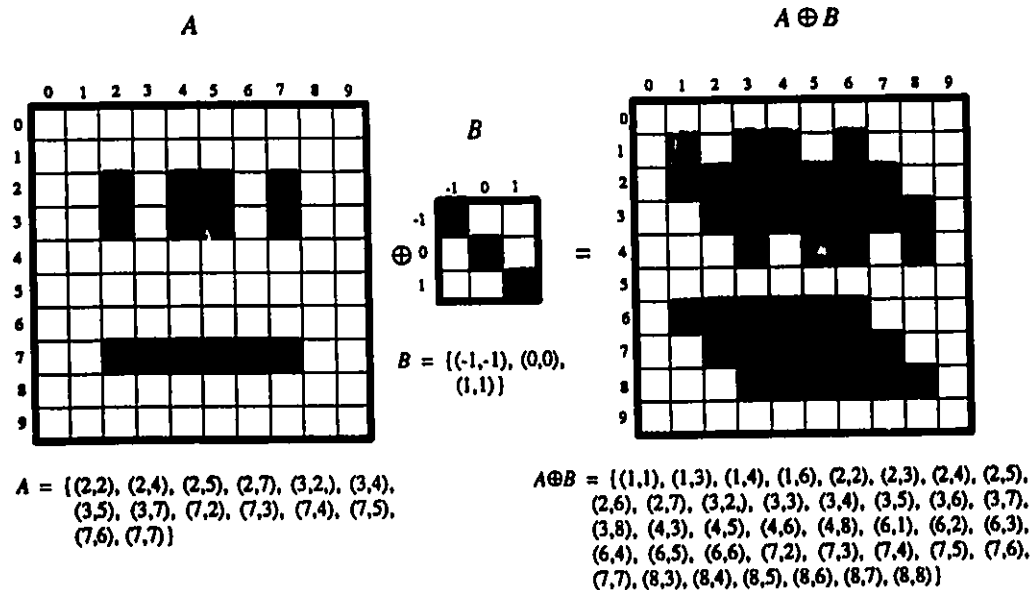


Fig. 3.1. Dilation of a binary image.

Since dilation incorporates vector addition, it exhibits associative, commutative, and distributive properties similar to that of addition. These and other properties of dilation are summarized in Table 3.1. Of particular interest is the associative and distributive properties. They permit dilations by large structuring elements to be computed as successive dilations and/or unions of dilations, by smaller structuring elements. For example, if a structuring element  $D$  can be expressed as the dilation of two smaller elements  $B$  and  $C$ , then the dilation of  $A$  by  $D$  may be evaluated by

$$A \oplus D = A \oplus (B \oplus C) = (A \oplus B) \oplus C. \quad (3.3)$$

**TABLE 3.1.**  
**PROPERTIES OF DILATION**

Property	Conditions	Description
Increasing	Yes	$A \subset B \Rightarrow A \oplus D \subset A \oplus B$
Extensive	iff B contains the origin	$A \oplus B \supset A$
Idempotent	No	—
Preserve Homotopy	No	—
Translational Invariance	Yes	$A \oplus B_x = (A \oplus B)_x$
Compatibility with Magnification	family	$\Psi_\lambda(A) = A \oplus \lambda B$
Associative	Yes	$A \oplus (B \oplus C) = (A \oplus B) \oplus C$
Commutative	Yes	$A \oplus B = B \oplus A$
Distributive	over unions	$A \oplus (B \cup C) = (A \oplus B) \cup (A \oplus C)$

This relation may be extended to  $k$  structuring elements in what is called the chain rule for dilation written

$$A \oplus (B_1 \oplus \dots \oplus B_k) = (\dots (A \oplus B_1) \oplus \dots \oplus B_k). \quad (3.4)$$

From the distributive property, if a structuring element  $D$  can be expressed as the union of two smaller elements  $B$  and  $C$ , then the dilation of  $A$  by  $D$  may be evaluated by

$$A \oplus D = A \oplus (B \cup C) = (A \oplus B) \cup (A \oplus C). \quad (3.5)$$

Equations (3.4) and (3.5) are used to decompose a dilation by a large structuring element into several smaller dilations. These techniques permit existing neighborhood connected image processors such as the Cytocomputer [29] to implement dilations larger than their neighborhood size. Papers by Zhuang and Haralick [30], and Pitas and Venetsanopoulos [31] are strictly devoted to the problem of morphological structuring element decomposition. However, not all structuring elements can be decomposed into a sequence of neighborhood dilations.

### ***C. Erosion***

The dual of dilation is erosion. The erosion of  $A$  by  $B$ , denoted  $A \ominus B$ , is defined as all the points  $c$  where the translates  $B_c$  are entirely contained in the image or

$$A \ominus B = \{c \mid B_c \subset A\}. \quad (3.6)$$

Erosion is also expressed as the intersection of translations of  $A$  by the elements  $-b$  where  $b \in B$ . Symbolically,

$$A \ominus B = \bigcap_{b \in B} A_{-b}. \quad (3.7)$$

Essentially, the structuring element is dragged across the image and only those points where the translated structuring element fits in the image remain. Fig. 3.2 illustrates the erosion of a binary image.

Erosion exhibits properties similar to those of dilation. These are summarized in Table 3.2. The associative and distributive properties again permit erosions by large structuring elements to be computed as successive erosions and/or intersections of erosions by smaller structuring elements. For example, if a structuring element  $D$  can be expressed as the dilation of two smaller elements  $B$  and  $C$ , then the erosion of  $A$  by  $D$  may be evaluated by

$$A \ominus D = A \ominus (B \oplus C) = (A \ominus B) \ominus C. \quad (3.8)$$

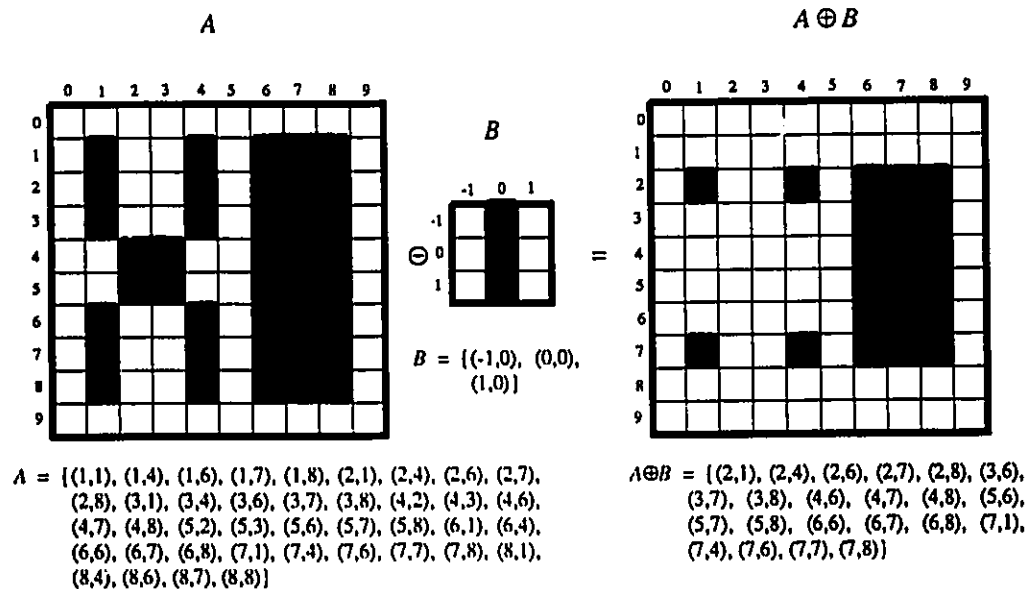


Fig. 3.2. Erosion of a binary image.

**TABLE 3.2.**  
**PROPERTIES OF EROSION**

Property	Conditions	Description
Increasing	Yes	$A \subset B \Rightarrow A \ominus D \subset A \ominus B$
Anti-extensive	iff B contains the origin	$A \ominus B \subset A$
Idempotent	No	—
Preserve Homotopy	No	—
Translational Invariance	Yes	$A_x \ominus B = (A \ominus B)_x$ $A \ominus B_x = (A \ominus B)_{-x}$
Compatibility with Magnification	family	$\Psi_\lambda(A) = A \ominus \lambda B$
Associative	with dilation	$A \ominus (B \oplus C) = (A \ominus B) \ominus C$
Commutative	No	$A \ominus B \neq B \ominus A$
Distributive	over unions	$A \ominus (B \cup C) = (A \ominus B) \cap (A \ominus C)$ $(A \cup B) \ominus C = (A \ominus C) \cap (B \ominus C)$

This relation may be extended to  $k$  structuring elements in what is called the chain rule for erosion, written

$$A \ominus (B_1 \oplus \dots \oplus B_k) = (\dots (A \ominus B_1) \ominus \dots \ominus B_k). \quad (3.9)$$

Likewise, if a structuring element  $D$  can be expressed as the union of two smaller elements  $B$  and  $C$ , then the erosion of  $A$  by  $D$  may be evaluated by

$$A \ominus D = A \ominus (B \cup C) = (A \ominus B) \cap (A \ominus C). \quad (3.10)$$

### ***D. Dilation Erosion Duality Theorem***

Eroding an image by a structuring element is equivalent to dilating the background of the image by the reflection of the structuring element. This is called the dilation erosion duality theorem and can be written as follows;

$$(A \ominus B)^c = A^c \oplus \overset{\vee}{B}, \quad (3.11)$$

where  $A^c$  denotes the complement of a set ,

$$A^c = \{x \in E^N \mid x \notin A\},$$

and  $\overset{\vee}{B}$  denotes the reflection of a set and is defined by

$$\overset{\vee}{B} = \{-b \mid b \in B\}$$

Figure 3.3 illustrates the duality theorem by eroding and dilating a binary image and its background respectively.

### ***E. Grey-Scale Morphology***

Grey-level images may be represented as sets on the 3-dimensional Euclidean grid  $E^3$ . The horizontal grid represents the spatial  $x,y$ -coordinates while the vertical  $z$ -coordinate represents the grey-level value or the height of the image surface. The set of image points is a thin sheet or surface which is expressed as a function  $f(x,y)$  of the spatial coordinates. In mathematical morphology, it is the umbra or shadow of this surface which is operated on. The umbra of a surface is illustrated in Fig. 3.4. It is the surface, and all the points below the surface defined by

$$U[f(x,y)] = \{z \mid z \leq f(x,y)\}.$$



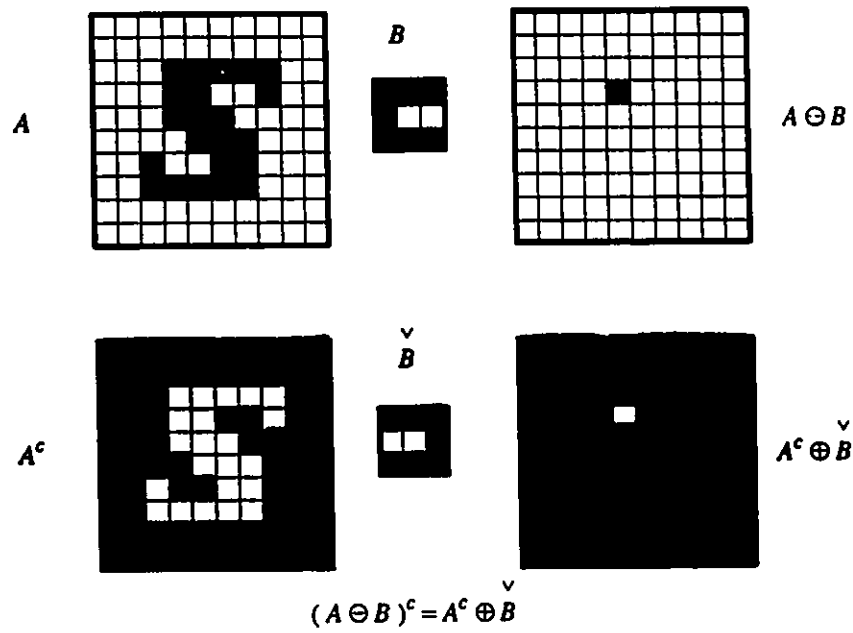


Fig. 3.3. Illustration of the dilation erosion duality theorem. At the top, the image  $A$  is eroded by the structuring element  $B$ . At the bottom the complement of  $A$  is dilated by the reflection of  $B$ .

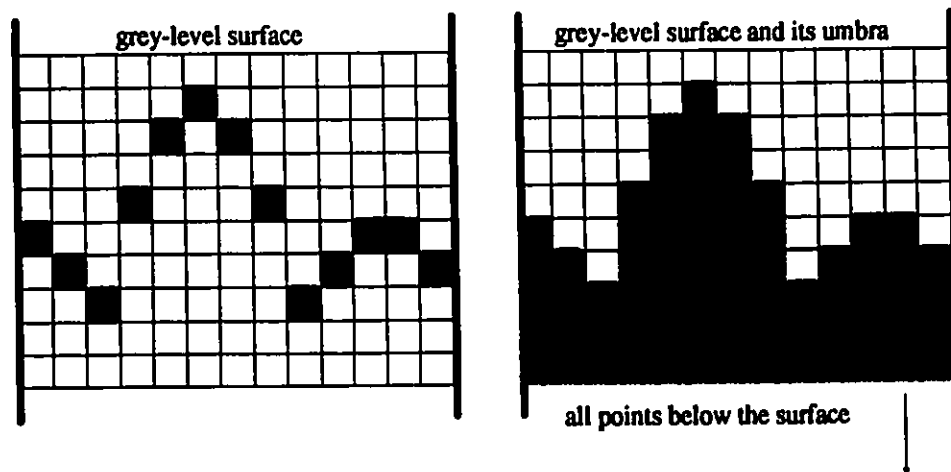


Fig. 3.4. The cross-section of a grey-level surface and the umbra of the surface.

The morphological transforms of dilation and erosion have been expressed as unions and intersections of sets. The union and intersection of umbrae are also umbrae. The union of two umbrae is the tallest of the two described by

$$U[x] \cup U[y] = U[\max(x,y)]. \quad (3.12)$$

The intersection of two umbrae occurs over the shortest of the two. Symbolically

$$U[x] \cap U[y] = U[\min(x,y)]. \quad (3.13)$$

Dilating or eroding an umbra by a structuring element also yields an umbra. That is

$$U[A \oplus B] = \bigcup_{b \in B} U[A]_b. \quad (3.14)$$

$$U[A \ominus B] = \bigcap_{b \in B} U[A]_{-b}. \quad (3.15)$$

The translation of the umbra of an image point  $A(x,y)$  by the point  $b=(i,j,B(i,j))$  is the umbra of the translated point  $A(x,y)_b$ . The  $(x,y)$  coordinates are translated by  $(i,j)$  while the grey-level value  $A(x,y)$  is translated by the grey-level value  $B(i,j)$ . Thus, the translation of an umbra is expressed mathematically as

$$U[A(x,y)]_b = U[A(x+i,y+j) + B(i,j)], \quad (3.16)$$

$$U[A(x,y)]_{-b} = U[A(x-i,y-j) - B(i,j)]. \quad (3.17)$$

Hence, the resultant at the coordinate  $(x,y)$  for the dilation or erosion of umbrae is computed as the union or intersection of image points translated from a distance  $(i,j)$ . Symbolically,

$$U[(A \oplus B)(x, y)] = \bigcup_{i, j \in B} U[A(x-i, y-j) + B(i, j)], \quad (3.18)$$

$$U[(A \ominus B)(x, y)] = \bigcap_{i, j \in B} U[A(x+i, y+j) - B(i, j)]. \quad (3.19)$$

Replacing the union of umbrae with the max operator, and the intersect of umbrae with the min operator yields

$$U[(A \oplus B)(x, y)] = \max_{i, j \in B} U[A(x-i, y-j) + B(i, j)], \quad (3.20)$$

$$U[(A \ominus B)(x, y)] = \min_{i, j \in B} U[A(x+i, y+j) - B(i, j)]. \quad (3.21)$$

Eliminating the umbra transform to express dilation and erosion in terms of the surface of the image yields

$$(A \oplus B)(x, y) = \max_{i, j} [A(x-i, y-j) + B(i, j)], \quad (3.22)$$

$$(A \ominus B)(x, y) = \min_{i, j} [A(x+i, y+j) - B(i, j)]. \quad (3.23)$$

Thus the erosion and dilation of grey-level images is reduced to min and max operations. The dilation and erosion of grey-level images is illustrated in Figures 3.5 and 3.6. The figures show a single scan line or cross section of an image being operated on.

Note that the umbra transform is often assumed when dealing with grey-level images. For example, when one specifies a grey-level image  $A$  and its complement  $A^c$ , it is understood that the complement is the area above the surface even though the umbra transform is not specified. Otherwise, by definition the complement  $A^c$  includes all the points above and below the thin surface  $A$ .

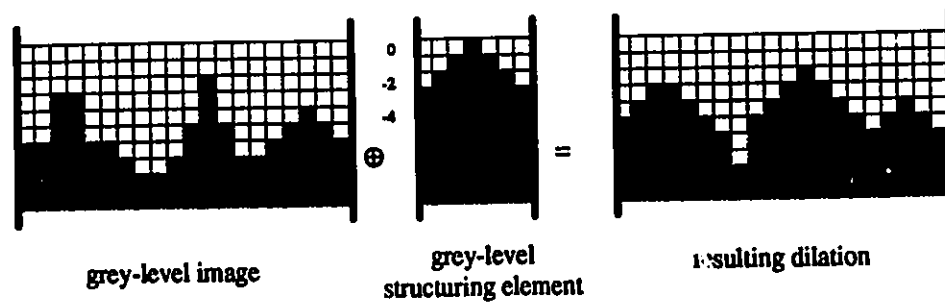


Fig. 3.5. Cross-sectional view of grey-level dilation.

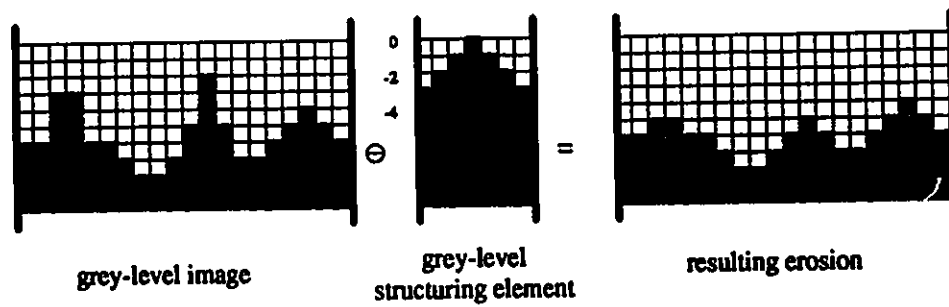


Fig. 3.6. Cross-sectional view of grey-level erosion.

## IV. SHAPE RECOGNITION ALGORITHM

At first glance, the morphological operation of erosion seems to be a good shape recognition tool. After all, the operation is used to find the points in an image where the structuring element is contained. Though erosion alone provides a necessary condition for shape detection it is not sufficient. In Fig. 4.1 the structuring element shown can either fit inside both the disk or the square though their shapes are different.

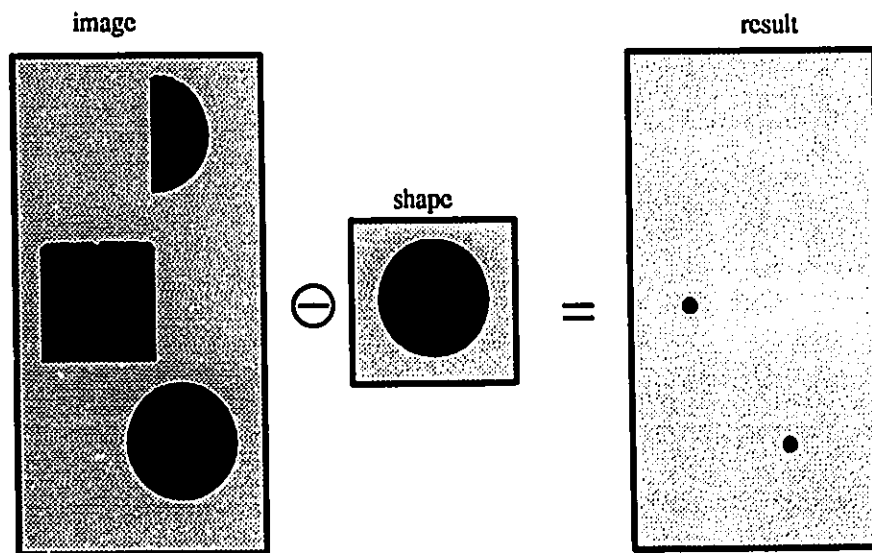


Fig. 4.1. The erosion of a binary image by a small disk. Notice that the result does not depend on the shape of the structuring element.

### A. The Generic Shape Recognition Algorithm

A stricter requirement for shape recognition is that the background of the structuring element also be present. This is the basis for the generic shape recognition algorithm introduced by Crimmins and Brown [17]. They satisfied both the foreground and background requirement with the following theorem.

*Theorem.*

The shape  $B$  defined in a window  $W$  occurs in the image  $A$  at the set locations  $C$  such that

$$C = (A \ominus B) \cap (A^c \ominus B^c), \quad (4.1)$$

where

$$B^c = W - B \quad (4.2)$$

The theorem is illustrated with the binary image of Fig. 4.2.

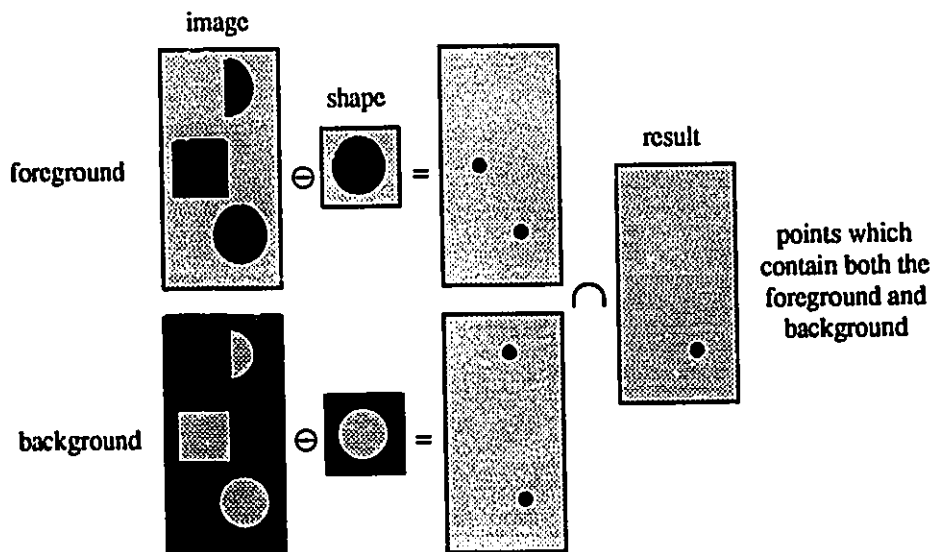


Fig. 4.2. The generic shape recognition algorithm applied to a binary image.

If the shape has variations or one wishes to locate rotated views of the object, then the shape recognition algorithm may be expanded to incorporate a family of shapes. Let  $B_\gamma$  describe the structuring elements where  $\gamma \in \Gamma$  is the family of variations of  $B$ . The shape  $B$  may then be found in an image  $A$  at the points  $C$  where

$$C = \bigcup_{\gamma \in \Gamma} [(A \ominus B_\gamma) \cap (A^c \ominus B_\gamma^c)]. \quad (4.3)$$

To adapt the recognition scheme of Crimons and Brown to the problem at hand, various changes and extensions had to be made. This work led to the new technique for shape recognition which is presented next.

### 1. The Grey-level Shape Recognition Algorithm

The extension to grey-level images requires again the use of the umbra transform. Figure 4.3 shows a vertical plot of one scan line through a grey-level image and structuring element.  $A \ominus B$  is traced by following the tip of  $B$  as  $B$  is dragged beneath the surface of  $A$ .  $A^c \ominus B^c$  is traced by dragging  $B^c$  above the surface of  $A$ . The intersection of the two erosions occurs where the lines representing the two erosions meet. However, if it is known that there is only one target in the scene, which is the case in this application, then the most likely location of  $B$  in  $A$  is where  $A \ominus B$  is closest to  $A^c \ominus B^c$ . Letting  $C(x, y)$  represent the shape recognition error function, then the most likely position of  $B$  in  $A$  is found at the minimum in  $C$  where  $C$  is the subtraction

$$C(x, y) = (A^c \ominus B^c)(x, y) - (A \ominus B)(x, y). \quad (4.4)$$

If more than one target was present in the scene, their positions could be estimated by considering all the minima below a threshold.

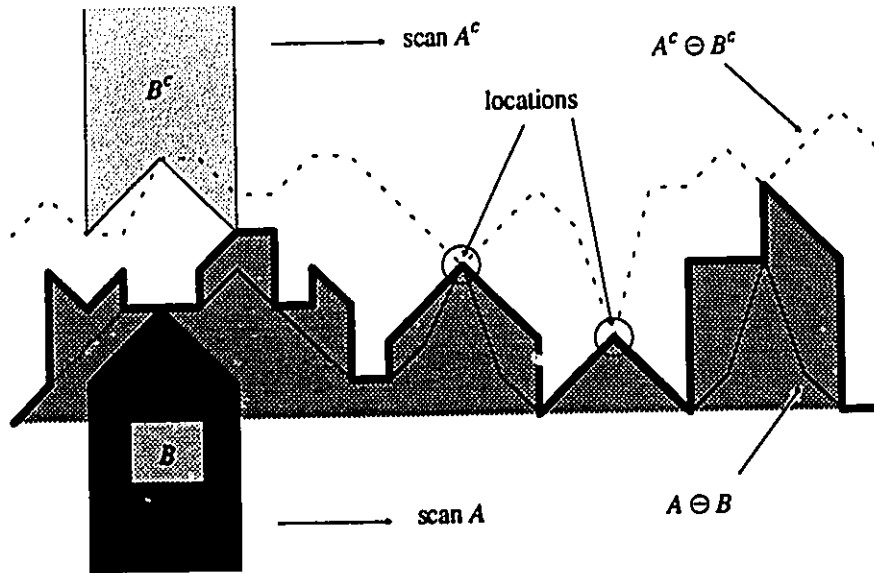


Fig. 4.3. The generic shape recognition algorithm applied to a cross section of a grey-level image.

Note again that for grey-level images the complements  $A^c$  and  $B^c$  are understood to be the complements of the umbrae  $U[A]$  and  $U[B]$  respectively.

The grey-level erosion  $A \ominus B$  has been derived in equation (3.23). The grey-level erosion  $A^c \ominus B^c$  is derived in a similar manner. From the dilation erosion duality theorem,

$$(U[A]^c \ominus U[B]^c)^c = U[A] \oplus \overset{\vee}{U[B]^c}. \quad (4.5)$$

From the definition of dilation

$$U[A] \oplus \overset{\vee}{U[B]^c} = \bigcup_{b \in \overset{\vee}{U[B]^c}} U[A]_b. \quad (4.6)$$



Reflecting the complement of the umbra of  $B$  is equivalent to taking the umbra of the reflection of  $B$  or

$$U[\check{B}]^c = U[\check{\check{B}}].$$

The union of  $U[A(x,y)]$  translated by the points in  $U[B(i,j)]$  overlap and are included in  $U[A(x,y)]$  translated by the surface point  $B(i,j)$ . Therefore, the umbra transform may be removed from the membership of the points  $b$  such that

$$U[(A^c \ominus B^c)^c] = \bigcup_{b \in \check{B}} U[A]_b = \bigcup_{b \in B} U[A]_{-b}. \quad (4.7)$$

This equation resembles the definition of erosion except the union operator is in place of the intersect. Substituting the union operator for the intersect operator in equation (3.19) leads to

$$U[(A^c \ominus B^c)^c(x,y)] = \bigcup_{i,j} U[A(x+i, y+j) - B(i,j)]. \quad (4.8)$$

The union operator may be replaced by the max operator, such that

$$U[(A^c \ominus B^c)^c(x,y)] = \max_{i,j} U[A(x+i, y+j) - B(i,j)] \quad (4.9)$$

Since the surface of  $U[A^c \ominus B^c]$  is the same as the surface of  $U[(A^c \ominus B^c)^c]$ ,

$$(A^c \ominus B^c)(x,y) = \max_{i,j} [A(x+i, y+j) - B(i,j)]. \quad (4.10)$$

Substituting this result and the grey-level equation for erosion into equation (4.4) yields the following grey-level shape recognition error function:

$$C(x,y) = \max_{i,j} [A(x+i, y+j) - B(i,j)] - \min_{i,j} [A(x+i, y+j) - B(i,j)]. \quad (4.11)$$

The following observation leads to an important modification to the algorithm. The operations  $A \ominus B$  and  $A^c \ominus B^c$  are very similar and differ only in that one uses the minimum while the other uses the maximum. Hence, the shape recognition algorithm which subtracts these two results, computes the max-min or the spread in the differences between the structuring element  $B$  and the window in the image  $A$  that  $B$  is overlapping during the scan. A problem with this algorithm is its susceptibility to noise. The problem is illustrated in Fig. 4.4. The extreme nature of using max and min operators causes the target to be missed, even though only one pixel is in error. The solution is to replace the max-min operation with a statistically more accurate representation of the spread. Experimentally, the standard deviation was found to provide such a

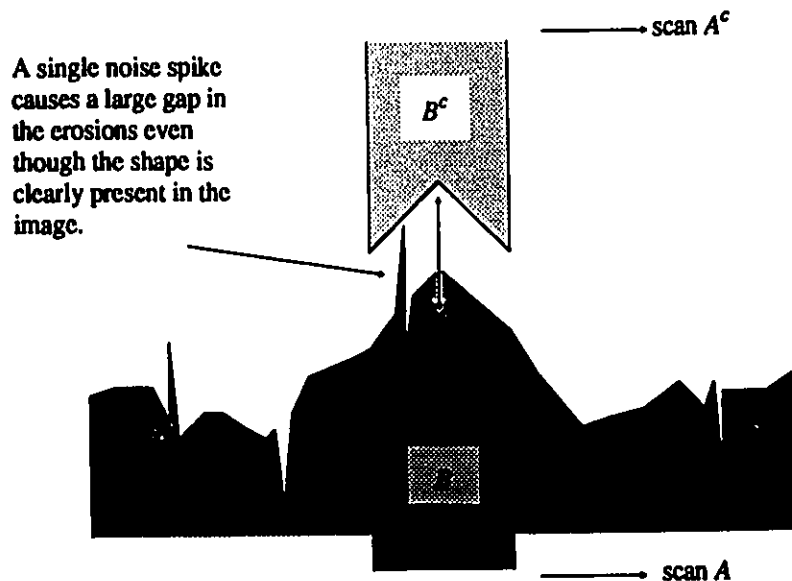


Fig. 4.4. The generic shape recognition algorithm applied to a corrupted image.

representation. Then the shape recognition error function  $C(x, y)$ , may be calculated from

$$C(x, y) = \text{STD}_{i,j} [ A(x+i, y+j) - B(i, j) ], \quad (4.12)$$

where STD denotes the standard deviation of a list of numbers and is calculated using

$$\text{STD}[ x_1, x_2, \dots, x_n ] = \frac{\sqrt{\sum x_i^2 - (\sum x_i)^2}}{n}. \quad (4.13)$$

The shape recognition error function calculated using equation (4.12) was found through experimentation to have some important advantages over that calculated using equation (4.11). First, it is less susceptible to noise spikes, which occur on cephalograms as scratches. Secondly, and more importantly, it provides room for minor variations in the shapes being located. If variations do occur, and the nature of this problem suggests that they will, then the statistical nature of equation (4.12) will provide a more confident result than would equation (4.11).

## **2. Decomposition**

The morphological shape recognition algorithm is not invariant to changes in scale and for precise shape recognition it should not be so. However, craniofacial landmarks are not precise and their sizes could vary considerably from patient to patient. One method of dealing with size differences is to decompose landmarks into small simple shapes. A complicated shape for which the algorithm is sensitive to scale may be broken down into smaller simpler shapes for which the algorithm is not as sensitive under scale differences. Figure 4.5a shows a shape which is located despite its size. In Fig. 4.5b the slightly more complex shape will not be located if it is a different size from the structuring element. Yet, if

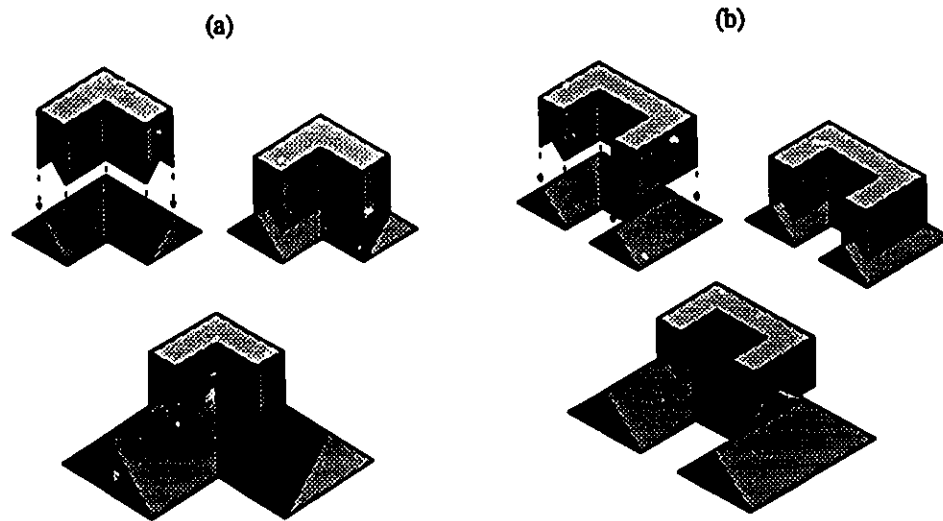


**Fig. 4.5.** An example of a shape which for varying sizes will (a) not pose a problem to the shape recognition algorithm, and (b) will be difficult to find with the shape recognition algorithm.

this shape was divided in two, then the separate halves could each be located despite the object size.

If a landmark is decomposed into several pieces or structuring elements, a method is required which combines the search results of each structuring element so that the minima in the separate shape recognition error functions overlap at the landmark centre. From the definition of erosion, the result from eroding  $A$  with the shape  $B$  will be translated to the defined origin of  $B$ . The result from the shape recognition error function, which is computed from erosions, will also be shifted to the origin of structuring elements. Thus the minima from more than one error function can be made to overlap at the landmark position by defining the origin of each structuring element to be the landmark's position.

Assume for the moment that the landmark is always of the same size. If the centre of the landmark is assigned as the origin for all the defining structuring elements, then their respective search minima will overlap at the landmark position. Let  $B_k$  denote the  $k$ th of  $n$  defining structuring elements for a landmark. Then the landmark location is found at the minimum of  $C_T$  where

$$C_T(x, y) = \sum_{k=1}^n \text{STD}_{i,j} [ A(x+i, y+j) - B_k(i, j) ] . \quad (4.14)$$

If the landmark in the image being searched is of a different size from that defined by the structuring elements, then the minima will not overlap. This is shown in Fig 4.6. In this tracing of the landmark sella, 3 structuring elements have been defined. The figure shows how the origins of the structuring elements overlap when the landmark is of the same size but do not overlap otherwise. What is needed is a more relaxed definition of the origins of the structuring elements.

Instead of defining a structuring element's origin as a point, assign a probability distribution to indicate the possible positions of the origin. A probability distribution may be trained to represent the location of the landmark centre with respect to each structuring element. Figure 4.7 illustrates how replacing the point origins with distributions allows the minima to overlap.

The idea demonstrated with the line drawings may be extended to grey-level images. Let  $L_k$  denote the location probability distribution of the origin of  $B_k$ . From here on  $L_k$  will be called the location distribution. Let  $C_k$  denote the shape recognition error function associated with the  $k$ th structuring element. The minimum or valley in  $C_k$  must be altered so that its shape is similar to that of  $L_k$ . Using mathematical morphology, which

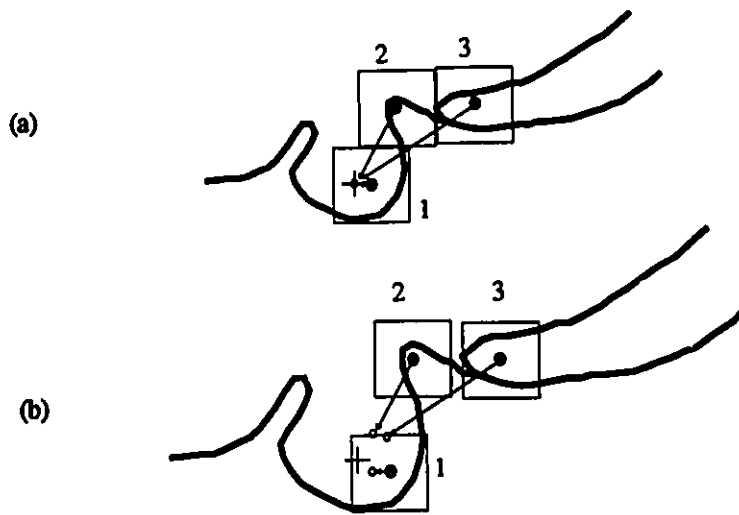


**Fig. 4.6.** A tracing of the landmark sella (a) decomposed into 3 structuring elements, and (b) the locations of these structuring elements on a larger version of the landmark.

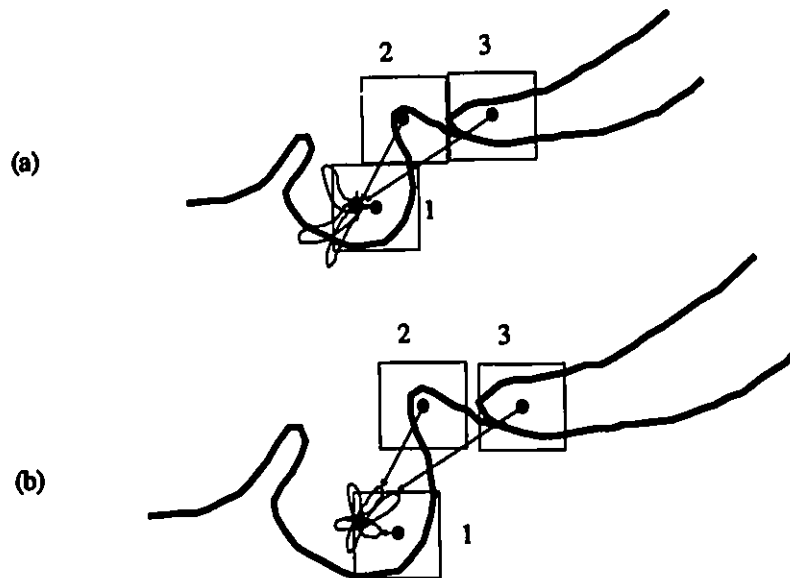


**Fig. 4.7.** Search results overlap in (a), and (b) when the point origins are replaced by probability distributions.

is ideally suited for dealing with shapes, this is done by dilating  $C_k^c$  by a scaled and inverted  $L_k$ . This is analogous to a dredging operation where a shovel with the shape of  $L_k$  enlarges the trenches and valleys in  $C_k$ , but never deepens them. Figure 4.8 illustrates how the location distributions are used to dredge the search results from two structuring elements such that their minimums overlap.

Let  $D_k$  denote the dredged shape recognition error function. Mathematically,  $D_k$  is evaluated by dilating  $C_k^c$  by the shape of  $L_k$  using

$$D_k = C_k^c \oplus \bar{L}_k. \quad (4.15)$$

where the inversion  $\bar{L}_k$  differs from the reflection  $\overset{\vee}{L}_k$  in that only the grey-level value is reflected. The spacial coordinates remain untouched.

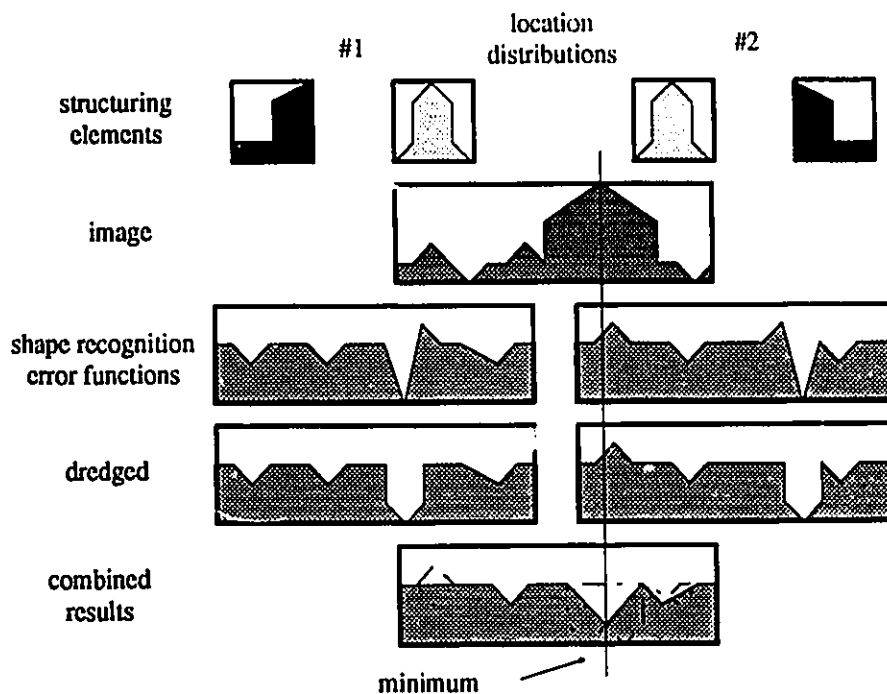


Fig. 4.8. Shape recognition applied to a grey-level landmark consisting of two structuring elements. Dredging is used to shape the minimums such that when combined they overlap.

To maximize its effect,  $L_k$  is scaled such that,  $1-n_g < L_k(x, y) \leq 0$  where  $n_g$  is the number of available grey-levels in the digitized x-ray images (in this case  $n_g = 256$ ). There are two reasons for this scaling. First, by shifting the distribution such that  $L_k(x, y) \leq 0$ , the origin of  $L_k$  is being shifted to the height of its peak. Consequently, when the image  $C_k$  is dilated by  $\bar{L}_k$ , the tip which is the origin will never affect points below it and thus the minimum will not be altered. Remember, the purpose of this dredging is to shape the valleys, not to make them deeper. Also, the values of the minima may prove of some use in assessing the strength of the find. Secondly, by altering the height of  $L_k$ , it is brought to scale with the error function  $C_k$ . Operating at the same scale maximizes the contrasting differences between shapes. For example, if  $-1 < L_k(x, y) \leq 0$  and  $-255 < C_k(x, y) \leq 0$  then operating on  $C_k$  by a different  $L_k$ 's would not be distinguishable.

The dredging operation expressed for grey-level images may be derived as follows. From the dilation erosion duality theorem

$$D_k = C_k \oplus \bar{L}_k = (C_k \ominus \check{L}_k)^c, \quad (4.16)$$

where  $\check{L}_k$  is  $L_k$  reflected in spatial coordinates only. That is

$$\check{L}_k = \{ l_{ij} \mid l_{ij} = L(-i, -j) \}. \quad (4.17)$$

Since the surface of an image and its complement are the same, the equation for grey-level erosion may be modified for the spatially reflected structuring element to yield the grey-level dredging operation

$$D_k(x, y) = \min_{i, j} [C_k(x-i, y-j) - L_k(i, j)] \quad (4.18)$$



The dredged error functions from more than one structuring element may then be summed to produce the combined error function from which the landmark location is extracted. Denoting  $D_T$  as the sum of the dredged error functions, the landmark location is found at the minimum where

$$D_T(x, y) = \sum_{k=1}^n D_k(x, y). \quad (4.19)$$

### 3. Summary

This new general shape recognition algorithm may be summarized as follows:

*Let  $B_k$  represent the  $k$ th of  $n$  structuring elements defining a landmark. Let  $L_k$  be the probability distribution representing the probable location of the origin with respect to the  $k$ th structuring element.*

The most likely location of the shape  $B$  in the image  $A$  is found at the minimum in the shape recognition error function  $D_T$  computed as the sum of the dredged error functions  $D_k$ . Symbolically,

$$D_T(x, y) = \sum_{k=1}^n D_k(x, y),$$

where  $D_k$  is computed using

$$D_k(x, y) = \min_{i,j} [C_k(x-i, y-j) - L_k(i, j)],$$

and  $C_k$  is the shape recognition function calculated from the  $k$ th structuring element using

$$C_k(x, y) = \text{STD}_{i,j} [A(x+i, y+j) - B_k(i, j)].$$

### 4. Locating the Minimum

The most likely location of the shape  $B$  in  $A$  is found by locating the minimum in the shape recognition error function  $D_T$ . When dealing with digital images, the minimum may not always be single valued or as shown in Fig. 4.9, it may not represent the centre of the valley. A more

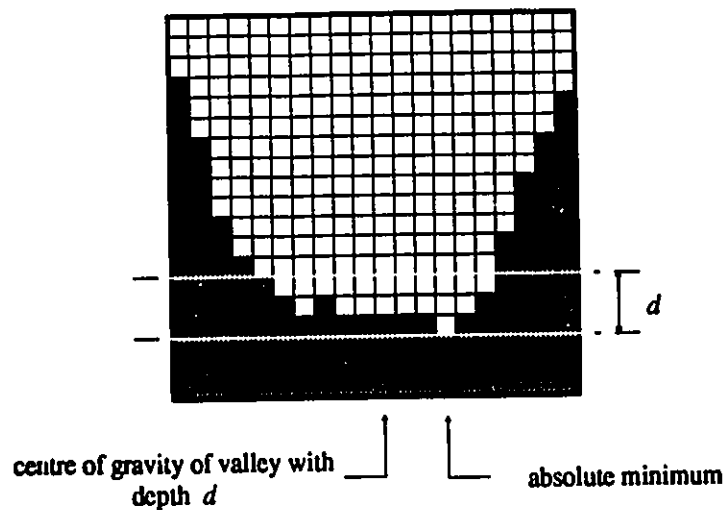


Fig. 4.9. Problems with locating the minimum in a digital image.

reliable method for determining the location of the minimum may be developed by using the centre of gravity. If one could imagine filling the valley with water up to a depth  $d$ , then the spatial centre of gravity of this body of water is a good representation for location of the minimum. The centre of gravity of a valley in a digital image may be found using the following algorithm:

*Let  $(x_{min}, y_{min})$  designate the location of the centre of gravity of the minimum with a depth  $d$ .*

1. Set  $d$  to some arbitrary value greater than 1, but not too large to avoid including points outside the local minimum in the computation.

2. Search for the value of the minimum in  $C$

$min = C(0,0)$

Scan all the points  $C(x,y)$  in  $C$

```

{
  if  $(C(x,y) < min)$ 
  {
     $min = C(x,y)$ 
  }
}

```

3. Compute the centre of gravity of the valley up to a depth  $d$

$x_{sum} = 0$

$y_{sum} = 0$

$n = 0$

Scan all the points  $C(x,y)$  in  $C$

{

  if ( $min \leq C(x,y) < (min + d)$ )

  {

$x_{sum} = x_{sum} + x (min + d - C(x,y))$    "weighted sum of x-coordinate"

$y_{sum} = y_{sum} + y (min + d - C(x,y))$    "weighted sum of y-coordinate"

$n = n + (min + d - C(x,y))$    "volume of valley"

  }

}

$x_{min} = x_{sum}/n$

$y_{min} = y_{sum}/n$

This algorithm assumes one global minimum. If there is more than one valley with points within the depth  $d$  of the global minimum, then those points may cause the centre of gravity to be located somewhere between the two local minimums. This effect may prove useful, though, if the dredging operation does not force the minima from separate shape recognition error functions to overlap completely. In such a situation the combined error functions may have neighboring local minima. It is more desirable then to select a position which is somewhere in between the minima than to select a location from only one of them.

### 5. Example

Using the landmark sella as an example, the following figures demonstrate the operation of this shape recognition algorithm. Sella is defined as the midpoint of the hypophysial fossa and is shown in Fig. 4.10. The landmark is shown decomposed into 3 structuring elements. Figure 4.11 shows the x-ray to be searched and the window to which the algorithm is to be applied. Figures 4.12 – 4.16 show the computed shape

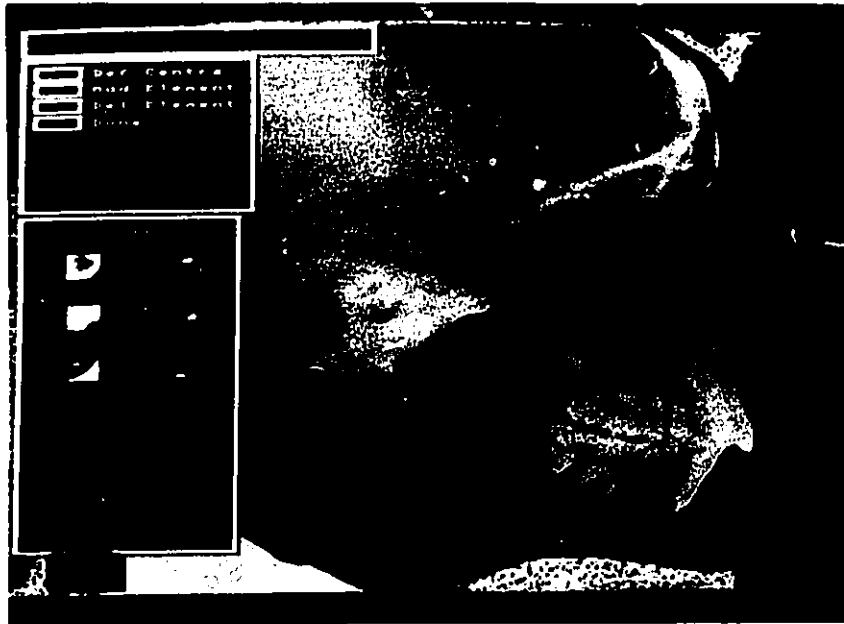


Fig. 4.10. A digital x-ray image of the landmark sella and its defining structuring elements.

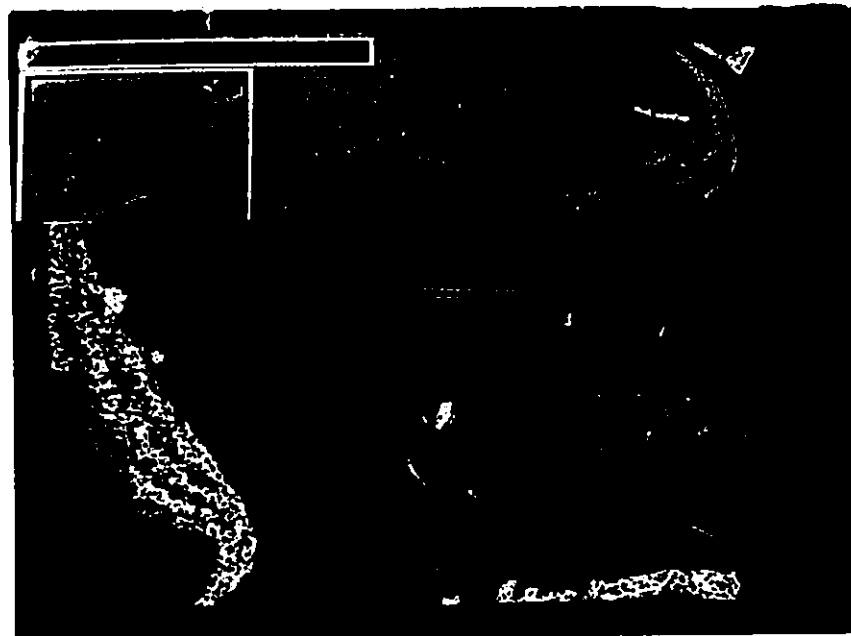


Fig. 4.11. An x-ray to be processed and the search window for locating sella.

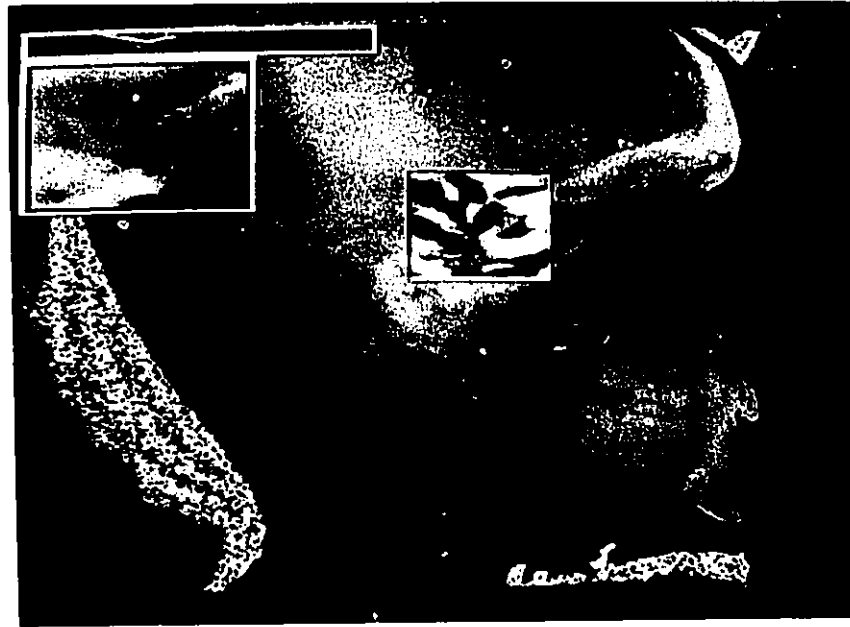


Fig. 4.12. The shape recognition error function when searching with the first structuring element.



Fig. 4.13. The shape recognition error function when searching with the second structuring element.

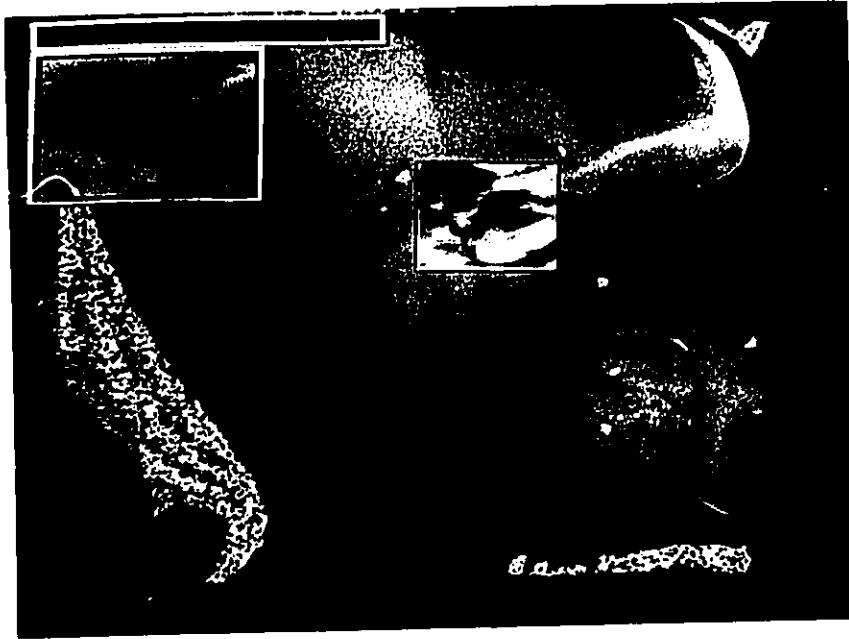


Fig. 4.14. The combined results from the first and second structuring elements.



Fig. 4.15. The shape recognition error function when searching with the third structuring element.

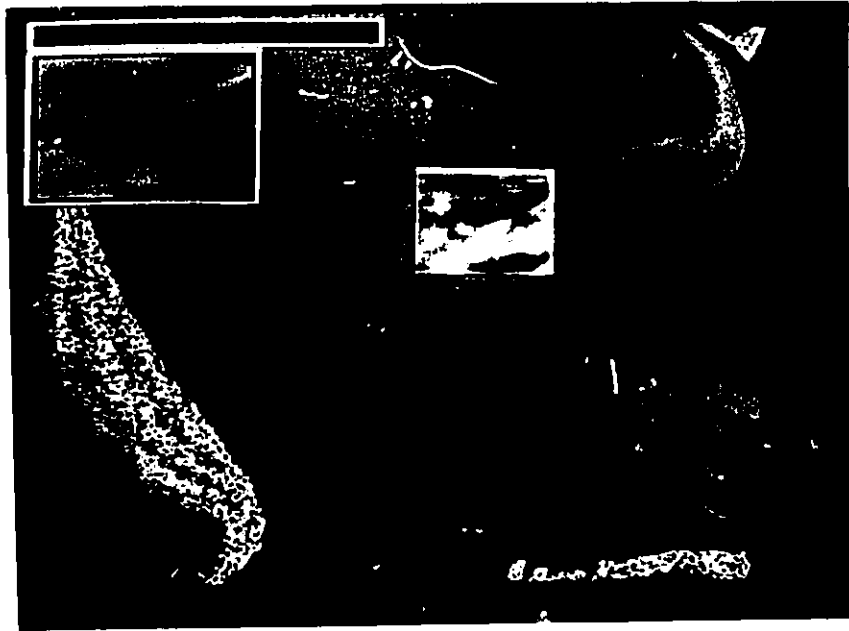


Fig. 4.16. The combined search results from all three structuring elements.



Fig. 4.17. The position of sella located at the minimum in the combined error function.

recognition error functions for each structuring element and the combined result. The minimum is located in Fig. 4.17.

### ***B. Training***

Training is required to define the structuring elements and their origins' location probability distributions. The procedure requires training data from x-rays with known landmark and structuring element locations. Supplying these positions by hand would be time consuming and prone to human-error. Instead, the shape recognition algorithm is used in localized searches to pinpoint the positions of individual structuring elements. Training data can then be extracted automatically from a newly processed x-ray whose landmarks have been located and verified.

Let the vector  $(x_k, y_k)$  denote the originally defined position of the  $k$ th structuring element with respect to the landmark's defined position. Given a newly processed x-ray with the  $i$ th landmark positioned at  $(px_i, py_i)$ , define the search window centre  $(swx_k, swy_k)$  for the  $k$ th structuring element at

$$\begin{aligned} swx_k &= px_i + x_k \\ swy_k &= py_i + y_k \end{aligned} \quad (4.20)$$

The search window size is set to the size of the maintained location distribution. There is no need to search beyond this region because even if a structuring element was found there, the maintained location distribution is not large enough to represent that find.

The shape recognition algorithm is applied to this window to locate automatically the  $k$ th structuring element. The procedure is illustrated in Fig. 4.18. Part (a) of the figure shows the located position of the landmark sella. In part (b) search windows are assigned to locate the structuring elements. In part (c) the shape recognition algorithm has



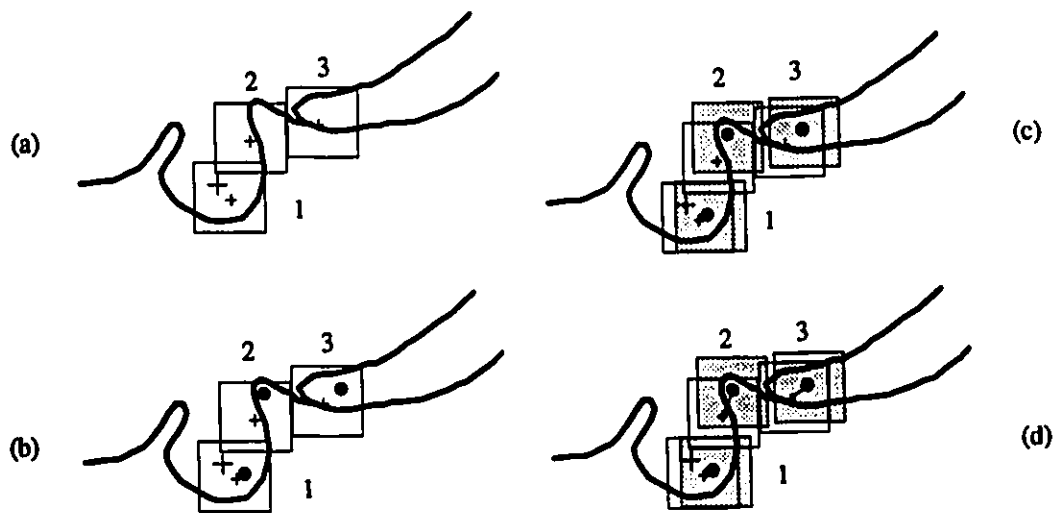


Fig. 4.18. Training the landmark sella by (a) assigned search windows for finding the structuring elements, (b) locating the positions of the structuring elements, (c) extracting training data from the located positions, and (d) using the difference in the located positions from the defined positions to update the location distribution.

located the structuring elements. If during a search the minimum falls on the boundary of the search window, there is a strong possibility that the structuring element was not in the search window. In this case, the training data should be ignored unless a larger location distribution is used. Finally part (d) shows the data taken for training. The procedure is summarized in the flow chart of Fig. 4.19.

### ***1. Updating the Structuring Element***

The exact shape of a structuring element will never be identical from x-ray to x-ray. To provide a balanced and equal representation for all x-rays, the structuring elements are trained using a cumulative average. Training data is extracted from each new x-ray as it is processed. First, the landmarks are located and their positions verified. Then the locations of the structuring elements are located automatically as described

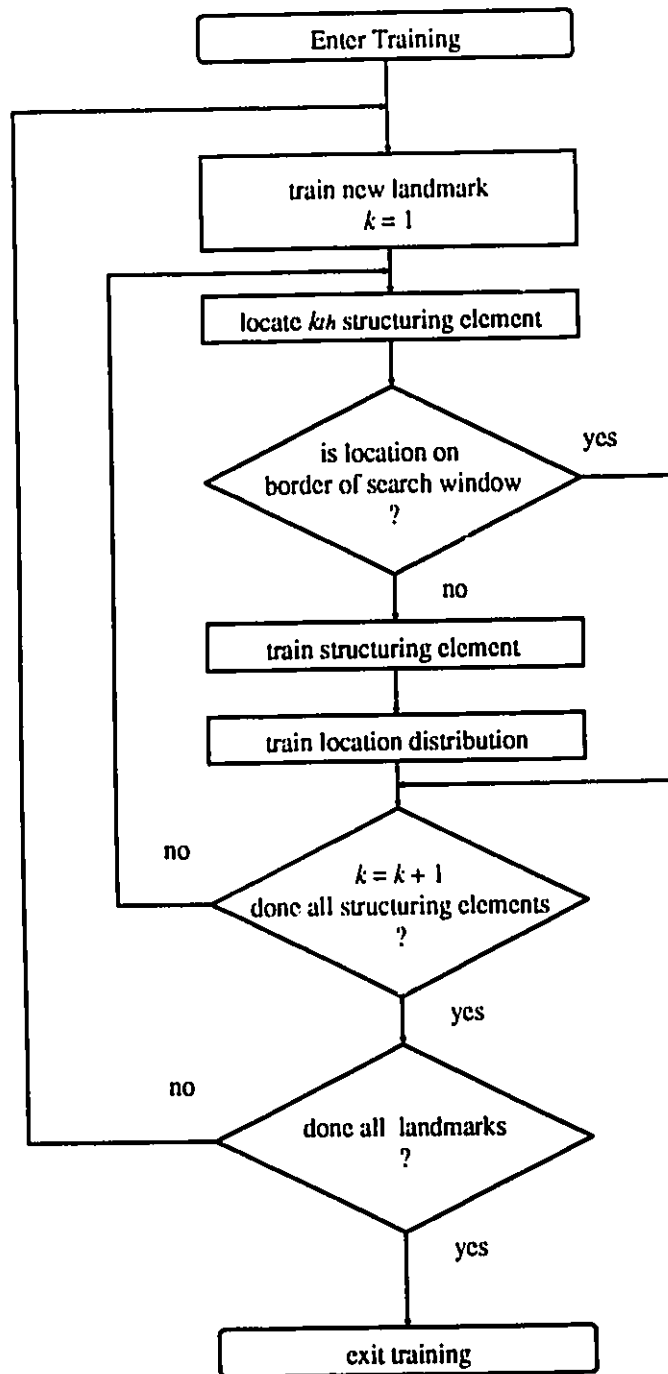


Fig. 4.19. Structuring element training procedure.

previously. Training data is then extracted from the x-ray at the found positions.

Let  $B_k^N$  represent the  $k$ th defined structuring element of a landmark which has been trained  $N$  times. Let  $B_k^i$  represent the new training sample taken from the newly processed x-ray. Then the structuring element is adjusted using.

$$B_k^{N+1}(i, j) = \frac{1}{N+1} [ N B_k^N(i, j) + B_k^i(i, j) ] . \quad (4.21)$$

If  $B_k^N$  is stored as a digital image with  $n_g$  grey-levels, then the training will not change  $B_k^N$  when  $N > (n_g - 1)$ . Training is no longer necessary beyond this point.

## **2. Updating the Location Distribution**

The location distribution is trained to reflect the relative position of the structuring element with respect to the landmark centre. The fixed vector  $(x_k, y_k)$  defines the initially assigned position of the structuring element. The distribution  $L_k$ , centered at a distance  $(-x_k, -y_k)$  from the  $k$ th structuring element, is trained to represent the probable location of the landmark when being located using that structuring element. Initially,  $L_k$  is assumed to be Gaussian shaped and centred at  $(-x_k, -y_k)$ . During training this distribution is updated by averaging Gaussian distributions with centres dictated by the training x-rays. Let  $(-x_k^i, -y_k^i)$  be the relative position of the  $k$ th structuring element on the training x-ray. The distribution, stored as an  $n \times m$  array, is updated by

$$L_k^{N+1}(i, j) = \frac{1}{N+1} \left[ N L_k^N(i, j) + \exp \left( \frac{((i+x_k-x_k^i-\frac{m}{2})^2 + (j+y_k-y_k^i-\frac{m}{2})^2)}{2\sigma^2} \right) \right] \quad (4.22)$$

The Gaussian is used instead of a spike for the reasons explained next. Figure 4.20 shows how averaging Gaussian humps leads to a smooth distribution faster than if averaging spikes. For a  $20 \times 20$  location distribution there are 400 possible locations to be trained. If these points were trained one at a time by averaging spikes, it would take over 400 x-rays before each point was adequately represented. By averaging Gaussians instead, every pixel is adjusted with each training x-ray. The resulting distribution is smooth and well representative after only a few (10-20) x-rays.

### 3. Example

Again, the landmark sella is used as an example, this time to demonstrate the automatic training algorithm. The located and verified position of the landmark on an x-ray to be used as training data is shown in Fig. 4.21. Figures 4.22, 4.23 and 4.24 show the computed shape recognition error functions for locating each of the 3 structuring elements in the vicinity of the landmark.

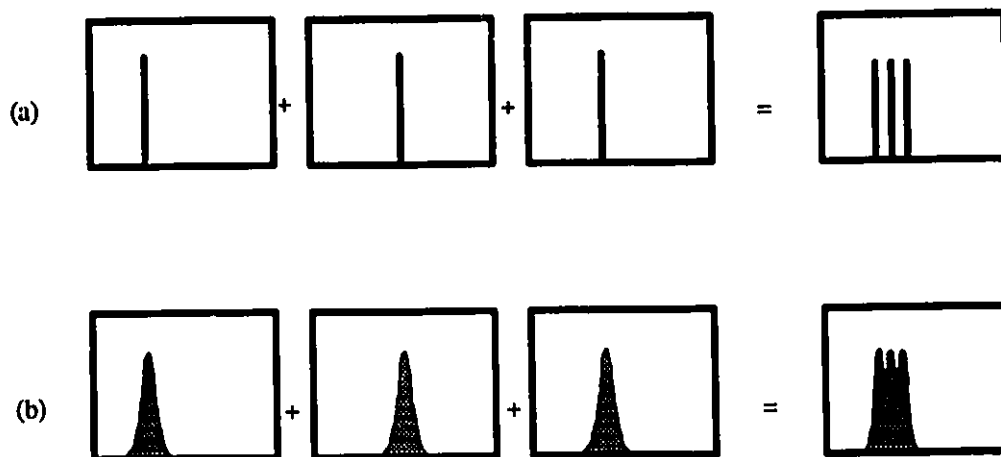


Fig. 4.20. Training the location distribution by averaging, (a) spikes and, (b) Gaussian distributions.



Fig. 4.21. The located and verified position of sella on an x-ray to be used for training.

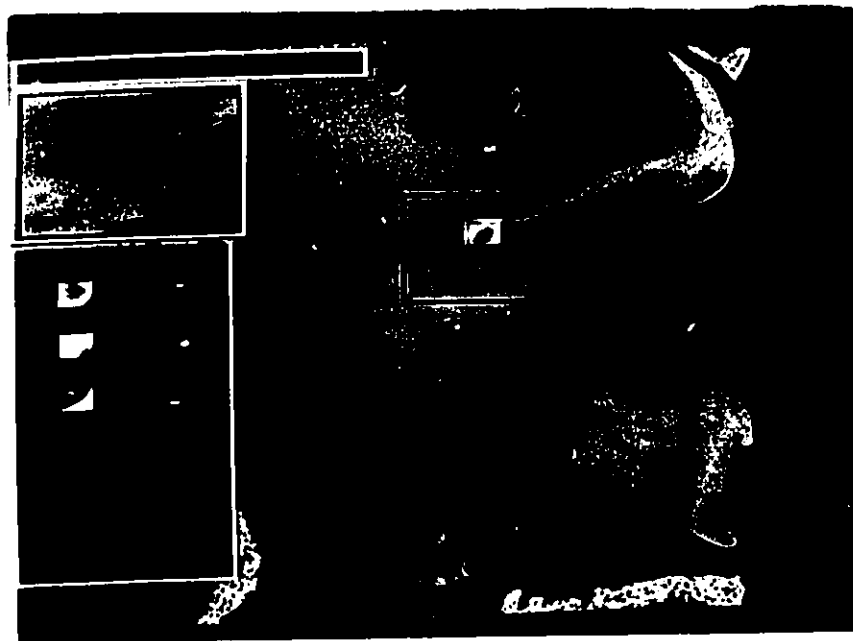


Fig. 4.22. The search results from the automatic training algorithm as it finds the first structuring element.

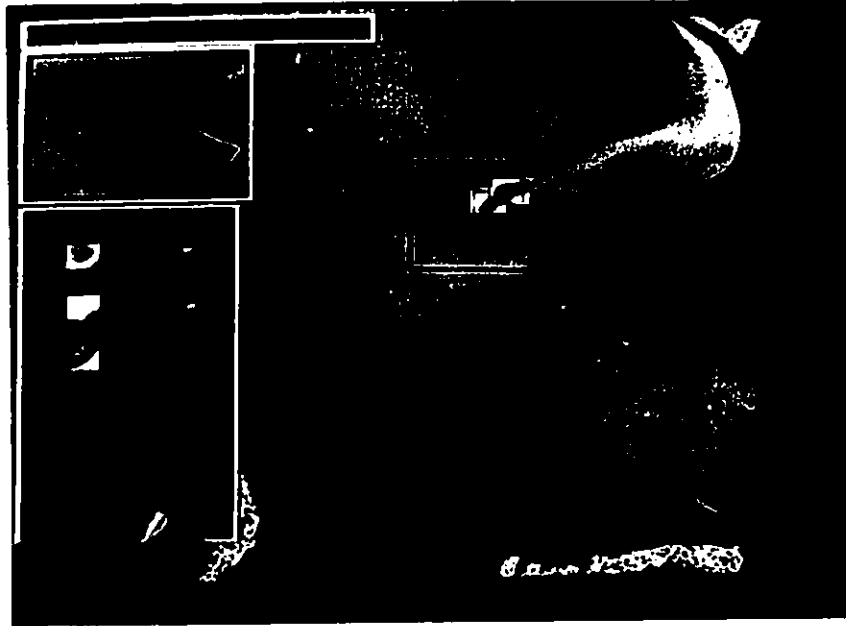


Fig. 4.23. The search results from the automatic training algorithm as it finds the second structuring element.

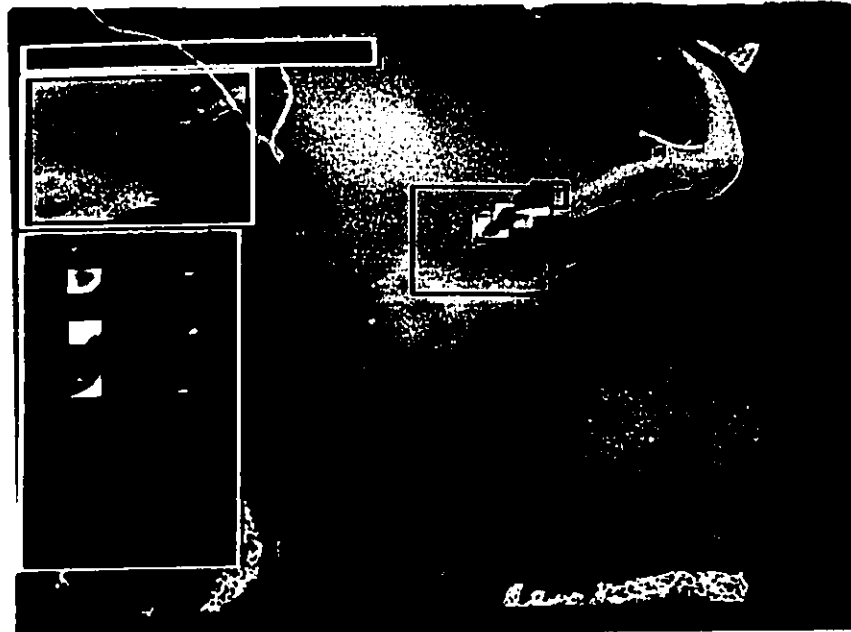


Fig. 4.24. The search results from the automatic training algorithm as it finds the third structuring element.

## V. SEARCH WINDOWS

Search window sizes are minimized to speed up the search and reduce the possible detection of false targets. This is done with a combination of training and removing of translational, rotational, and size differences between x-rays during the locating process.

Each x-ray differs somewhat in size, placement and tilt. There are obvious shape differences as well, but the mentioned transformations may be easily compensated for and removed from the effective search space. In effect, as points are being located, the positions of subsequent landmarks are more accurately predicted. Thus the required search window sizes decrease from landmark to landmark. Due to the nature of some landmarks, this reduction in search window size is not consistent. For example, the tips of the incisors are much more capable of moving than the bridge of the nose. Therefore, it should be reasonable to expect a larger search window for locating the incisors after having located the bridge of the nose. Even so, the required search window sizes will always be smaller with translational, rotational and size differences removed.

Figure 5.1 demonstrates how the defined search windows are transformed so that the implemented search windows are as close to the landmark positions as possible. The reference x-ray in part (a) of the figure shows the expected positions of nasion and pogonion with respect to sella. Parts (b) and (d) show the large window sizes which would be required to locate nasion and pogonion. In parts (c) and (e) the required window sizes have been drastically reduced by removing the translational, rotational and size difference between the reference x-ray and the target

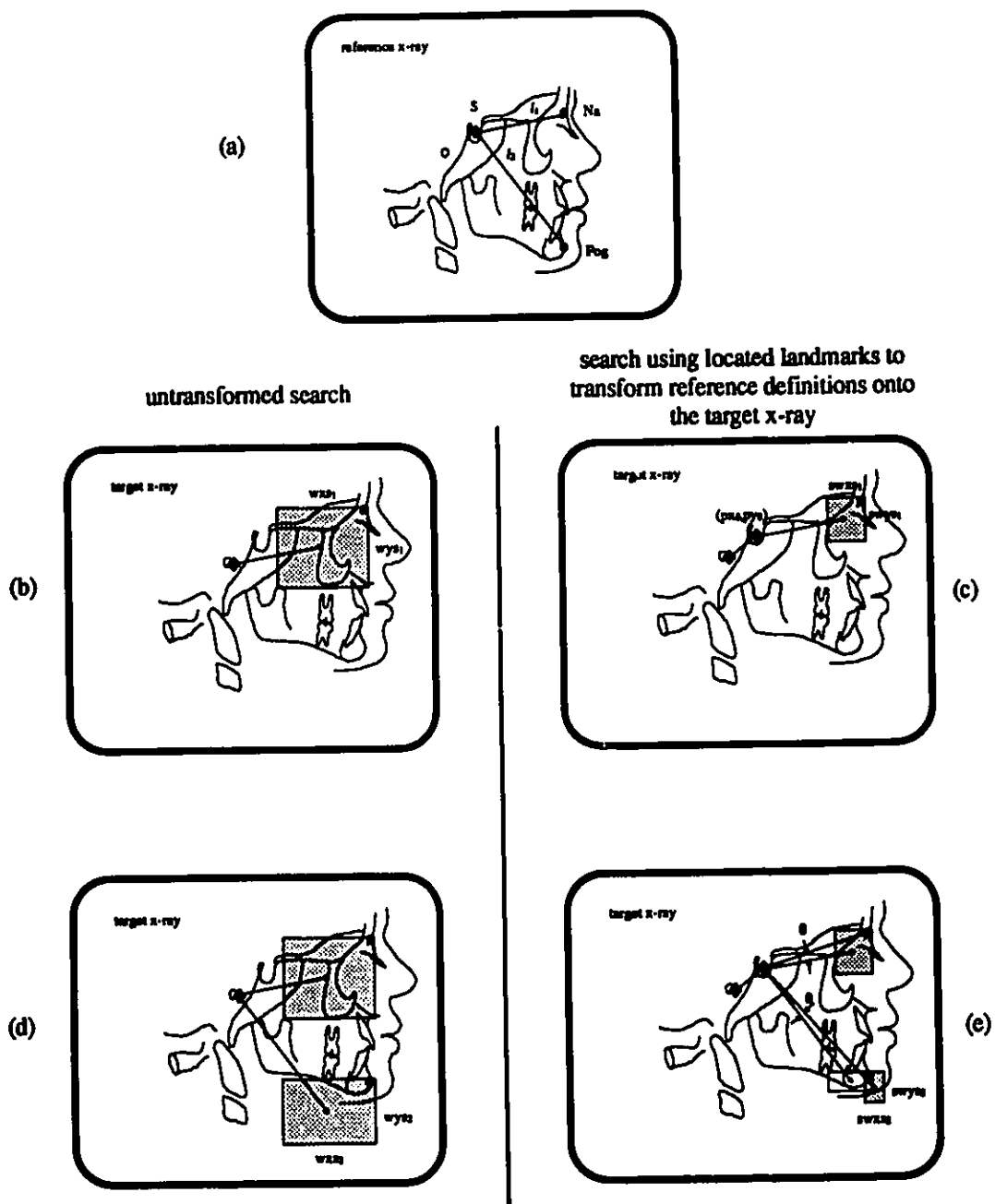


Fig. 5.1. Transforming defined search windows onto the target x-ray. (a) Reference x-ray. (b) Required search window to find Na. (c) Require search window to find Na using S to remove translational difference. (d) Required search window to find Pog. (e) Required search window to find Pog using S and Na to remove translational, rotational and size differences.



x-ray. This was done by using the previously located position of sella to translate the window centres and using the second located landmark nasion to estimate the rotational and size differences.

Note that what has been shown is that the required window sizes will be smaller if translational, rotational, and size differences are compensated for. To make use of this idea two separate steps are required. First, a technique must be developed which compensates for and removes these transformations during the search. The technique should make use of located points to estimate the transformational differences between a trained reference x-ray and the x-ray being processed. Second, a training method needs to be developed for learning the smaller required window sizes and maintaining a definition of them with respect to the reference x-ray. First, consider the problem of estimating the transformational differences between the reference x-ray and the x-ray being processed.

#### ***A. Estimation of Translational, Rotational and Size Differences***

Let  $(wx_i, wy_i)$  and  $(wxs_i, wys_i)$  denote the defined window centre and size for the  $i$ th point. These are initially defined on the reference x-ray. They are then trained to represent subsequently processed x-rays. Let  $(px_i, py_i)$  denote the position of the  $i$ th landmark on the x-ray being processed. Let  $(swx_i, swy_i)$  and  $(swxs_i, swys_i)$  denote the search window centre and size used to locate the position of the  $i$ th landmark on the x-ray being processed.

Denote the transformation  $T$  as a  $[2 \times 1]$  translation matrix and  $R$  as a  $[2 \times 2]$  square transformation which performs rotations and scaling. It is not necessary to maintain a separate  $[2 \times 2]$  rotation matrix and  $[2 \times 2]$  scaling matrix since the two may be concatenated using matrix multiplication. When locating the first landmark neither  $T$  nor  $R$  is known.

Consequently, the first search window cannot be minimized during training and thus must be large enough to account for these possible transformational differences between x-ray images. The location of the first point provides the translation matrix  $T$ . The elements of the  $[2 \times 2]$  matrix  $R$  may be estimated one column at a time using the method of least squared error, but not until 2 more landmarks have been found. The positions of two additional landmarks is the minimum amount of data necessary to solve for 2 unknowns in the least squares fit. The procedure is summarized in the following algorithm:

1. Initialize the rotation matrix to the Identity matrix.

$$R = I$$

2. Set  $i=0$ . Set the search window centre and size for the 0th point.

$$\begin{aligned} swx_0 &= wx_0 & swxs_0 &= wxs_0 \\ swy_0 &= wy_0 & swys_0 &= wys_0 \end{aligned}$$

3. Find the location of the point  $(px_0, py_0)$ . Adjust the translation matrix  $T$  such that this location is the origin of the search space.

$$T = \begin{bmatrix} px_0 \\ py_0 \end{bmatrix}.$$

4.  $i = i + 1$ .

Locate the next point as follows:

5. Calculate the search window centre and size using;

$$\begin{aligned} \begin{bmatrix} swx_i \\ swy_i \end{bmatrix} &= R \begin{bmatrix} wx_i - wx_0 \\ wy_i - wy_0 \end{bmatrix} + T, \\ \begin{bmatrix} swxs_i \\ swys_i \end{bmatrix} &= R \begin{bmatrix} wxs_i \\ wys_i \end{bmatrix}. \end{aligned}$$

6. Apply the shape recognition algorithm to find the location of the  $i$ th point  $(px_i, py_i)$ .

7. If  $(i \geq 2)$  adjust the rotation/scaling matrix  $R$  using least squares. Ideally, the landmark position would be at the transformed window centre,

$$\begin{bmatrix} px_i - px_0 \\ py_i - py_0 \end{bmatrix} = R \begin{bmatrix} wx_i - wx_0 \\ wy_i - wy_0 \end{bmatrix}.$$

Let

$$W^T = \begin{bmatrix} wx_1 - wx_0 & wx_1 - wx_0 \\ wx_2 - wx_0 & wx_2 - wx_0 \\ \vdots & \vdots \\ \vdots & \vdots \\ wx_i - wx_0 & wy_i - wy_0 \end{bmatrix},$$

$$P^T = \begin{bmatrix} px_1 - px_0 & px_1 - px_0 \\ px_2 - px_0 & px_2 - px_0 \\ \vdots & \vdots \\ \vdots & \vdots \\ px_i - px_0 & py_i - py_0 \end{bmatrix}.$$

Then  $\mathbf{R}$  is solved using least squares or,

$$W^T W R^T = W^T P$$

8. If ( $i < \text{number of points}$ ) go to 4, else stop.

This algorithm describes how to estimate the transformational differences between the reference x-ray containing the search window definitions and the x-ray being processed. What is required to complete this idea is a training scheme that will figure out the required window sizes when using this scheme.

### ***B. Window Training***

Similar to the way the defined search window centres and sizes were transformed from the reference x-ray onto the x-ray being processed using the estimated transformation matrix  $\mathbf{R}$ , the located landmark positions may be transformed back onto the reference x-ray for training using the inverse transform  $\mathbf{R}^{-1}$ . It is through this inverse transformation that the translational, rotational and size differences are removed and the window sizes are minimized. The search window centres are trained by averaging the transformed positions of the located landmarks. The window sizes are trained by calculating the minimum required size from the distance between the defined window centre and the located landmark position. The window sizes are initially set to some arbitrary value. Averaging

subsequent minimum required sizes allows the window size to shrink or be minimized. If a required window size should ever be greater than the currently defined size, then that size must take precedent to ensure that the landmarks fall within the search windows in future x-rays. The search windows are adjusted according to the following algorithm.

Let  $N$  be the number of x-rays trained.

1. Set  $i=0$ .
2. Use the first landmark location as training data.

$$wx_0^f = px_0,$$

$$wy_0^f = py_0.$$

3. The window centre  $(wx_i^N, wy_i^N)$  is adjusted using a cumulative average as follows;

$$wx_i^{N+1} = \frac{N wx_i^N + wx_i^f}{N+1},$$

$$wy_i^{N+1} = \frac{N wy_i^N + wy_i^f}{N+1}.$$

4. The search window size  $(wsx_i^N, wsy_i^N)$  is adjusted by first computing the minimum required window size  $(wsx_i^f, wsy_i^f)$  using

$$wsx_i^f = |wx_i - wx_i^f| + wsx^s$$

$$wsy_i^f = |wy_i - wy_i^f| + wsy^s$$

where  $(wsx^s, wsy^s)$  is an arbitrary safety margin. The sizes are then adjusted as follows;

if  $(wsx_i^f > wsx_i^N)$  "expand"

$$wsx_i^{N+1} = wsx_i^f,$$

else "contract"

$$wsx_i^{N+1} = \frac{N wsx_i^N + wsx_i^f}{N+1}.$$

if  $(wsy_i^f > wsy_i^N)$  "expand"

$$wsy_i^{N+1} = wsy_i^f,$$

else "contract"

$$w_{sy_i}^{N+1} = \frac{N w_{sy_i}^N + w_{sy_i}^i}{N+1}.$$

5. Train the next point,  $i = i + 1$ .
6. If ( $i > \text{number of points}$ ) stop.
7. Transform the landmark location to remove the translational, rotational and size differences. The transformed points are calculated by

$$\begin{bmatrix} wx_i^i \\ wy_i^i \end{bmatrix} = \mathbf{R}^{-1} \begin{bmatrix} px_i - px_0 \\ py_i - py_0 \end{bmatrix} + \begin{bmatrix} wx_0 \\ wy_0 \end{bmatrix},$$

where the transformation matrix  $\mathbf{R}$  is estimated using least squares as described in the previous algorithm. The matrix  $\mathbf{R}$  must be estimated using only the landmark locations before the  $i$ th point. The transformations must be applied consistently during the search and during training in order for the training to be effective.

8. Go to 2.

This completes the search window minimization technique. The transformation matrix  $\mathbf{R}$  which is estimated in the first algorithm may be also put to use in the shape recognition algorithm.

### ***C. Transforming the Structuring Element Positions***

For each landmark, the  $k$ th structuring element is given a fixed vector  $(x_k, y_k)$  to define its position about the landmark and to define the position of the location distribution  $L_k$ . Since these landmark and structuring element definitions are maintained on the same reference x-ray as are the window definitions, the estimated transformation  $\mathbf{R}$  may be also applied to the landmark definitions. Any estimated rotational and scale differences between the reference x-ray and the x-ray being processed may be removed from the landmark definitions to some extent by transforming the fixed vector  $(x_k, y_k)$ . This vector may be transformed by

$$\begin{bmatrix} x'_k \\ y'_k \end{bmatrix} = \mathbf{R} \begin{bmatrix} x_k \\ y_k \end{bmatrix}. \quad (5.1)$$

This transformed vector may be applied both during the application of the shape recognition algorithm and during the structuring element training. Applying it during the training may produce slightly sharper location distributions with the transformational differences removed.

## VI. EXPERIMENTAL RESULTS

The desired outcome of this research is a complete cephalometrics workstation. The minimum hardware requirements for the system are a personal computer, a frame grabber, camera, and backlight or equivalent for digitizing the cephalograms, and a graphics display capable of displaying  $512 \times 480$  digital 256 grey-level images. Preferably, the developed software should be hardware independent for easy transportability. To be competitive, the system must be able to provide an error free analysis of an x-ray within approximately 10 minutes. Current systems using digitizing tablets require about 10 minutes to load the landmark locations manually. The ideas and algorithms developed in this research were implemented and tested with these goals in mind.

The shape recognition algorithm was implemented on the system shown in Fig. 6.1. It consists of an IBM-AT running at 8 MHz, an EGA color graphics card and monitor, a mouse, a four quadrant frame grabber with room for 4  $512 \times 512$  256 grey-level images, a video camera and backlight.

A total of 20 assorted landmarks was selected from the Atlas of Cephalometry [1] for the experiments. The landmarks were of varying types and should provide an adequate test base for assessing this shape recognition algorithm. A better than average radiograph was used as a reference x-ray. This x-ray provided data for the initial landmark and search window definitions. The landmarks were defined by a centre and up to 6  $20 \times 20$  structuring elements. For each structuring element a  $20 \times 20$  location distribution was also initialized. Table 6.1 lists the selected



Fig. 6.1. The cephalometrics work station.

landmarks and the number of structuring elements used to define each landmark. They are listed in the order in which the locating algorithm was applied. Figure 6.2 shows the locations of these points on the reference x-ray.

The algorithm was tested on 40 randomly selected x-rays of male and female patients ranging from 9 to 39 years of age. Two sets of tests were performed. In the first set, the algorithm attempts to locate the landmarks on new x-rays. Training is performed after processing each x-ray. This set of tests provides an assessment of the algorithm's ability to learn. Whether the algorithm's success rate improves with training is shown here. The second set of tests evaluates the system's long term performance when training is no longer necessary. The 40 x-rays are processed again. The system is thus presented with familiar shapes



**TABLE 6.1.  
DEFINED TEST LANDMARKS**

No.	Landmark	Abbreviation	structuring elements
1	Sella	S	3
2	Nasion	Na	3
3	Menton	Me	2
4	Gonion	Go	4
5	Porion	Po	1
6	Posterior point for the occlusal plane	PPOcc	1
7	Anterior point for the occlusal plane	APOcc	3
8	Posterior nasal spine	PNS	3
9	Anterior nasal spine	ANS	3
10	Pogonion	Pog	2
11	Gnathion	Gn	2
12	Orbitale	Or	3
13	Incisor superior	Is $\perp$	2
14	Incisor inferior	Is $\bar{1}$	3
15	Apicale $\perp$	Ap $\perp$	2
16	Apicale $\bar{1}$	Ap $\bar{1}$	2
17	Point A, subspinale	A	2
18	Point B, supramentale	B	2
19	Soft tissue pogonion	Soft Pog	3
20	Tip of the Nose	Nose	3



**Fig. 6.2.** The test landmarks used in the experiments.

encountered during previous training sessions. This resembles the state of the system when the training has converged and is no longer necessary. This provides some assessment of the long term performance and capability of this system.

The lateral skull x-rays are  $245 \times 190$  mm in size and are digitized to a resolution of  $512 \times 490$  pixels and 256 grey-levels. With this resolution, position accuracies of about 0.5mm at best are possible. This resolution is more than adequate considering that the accepted normal range of most measurements is roughly  $\pm 2$ mm [1].

Test results are obtained by verifying the located positions of the landmarks by hand. The distance in mm between the computer located position and the operator specified position is recorded as the location

error of the algorithm. The verified positions are then used for training so that the system will learn the operator's preferences. This is desirable since most orthodontists have different ideas about the best defined position for various landmarks.

The best possible accuracy to be expected of this system depends on the repeatability of the operator. If presented with the same x-ray, to what accuracy will the observer repeatedly point out the same landmark? In these experiments the operator was able to repeat positions to within 2 pixels or  $\pm 1\text{mm}$ .

### ***A. Experiment 1 — Locating Before Training***

#### ***1. Purpose***

The purpose of this experiment is to assess the performance of the shape recognition algorithm during training.

#### ***2. Procedure***

The system is initialized with the definitions of the 20 test landmarks. X-Rays are then processed. The algorithm is applied first to locate the landmarks. The operator then verifies those locations, recording the distance error for each landmark. Distance errors for landmarks which were not within the search window are not recorded since the chances of locating that landmark were zero to begin with. After verifying landmark positions and recording the results of the search the automatic training algorithm is allowed to proceed. This is repeated for all 40 x-rays.

#### ***3. Observations***

The results have been summarized in Table 6.2. This table lists the location errors for each landmark, the time required to process each x-ray, and a categorized summary of the results. The summary has grouped the

**TABLE 6.2.**  
**LOCATION ERRORS FOR EXPERIMENT #1 (mm)**

x-ray			landmark															time hrs:min	summary				% of points in search windows								
																			points < 2mm	points 2 - 5 mm	points > 5mm	not in window			% < 2mm	% 2 - 5mm					
No.	Age	Sex	Se	Na	Me	Go	Fo	POcc	AOcc	PNS	ANS	Pog	Gn	Or	Is I	Is I	Ap I	Ap I	A point	B point	Soft Pog	Tip of Nose									
1	9	F	6.5	1.9				0.4				0.9	1.6				1.6		8.0	1.0	3.4		4:44	6	1	2	11	66	77		
2	10	F	5.4																			4.2		3:13	0	1	1	18	0	50	
3	10	F	0.4	1.0	1.1	0.2	0.0	6.0	3.0	2.4	1.8	1.5	1.5	3.0	4.1	2.2	2.5	0.7	2.1	1.8	1.0		2:31	11	7	1	1	38	94		
4	10	F	1.4	1.5	6.8	10.0	0.6	2.8	2.4	2.5	4.9	0.0	4.5	3.1	0.0	0.4	0.0	3.0	0.6	1.3	0.0		2:14	10	7	2	1	53	89		
5	11	M	3.8	0.3	2.9	0.4	0.5	3.9	5.7	3.0	0.0	1.4	1.8	0.8	0.2	1.9	1.4	3.0	0.0	1.5	1.2	1.0		2:38	15	3	2	0	75	90	
6	11	F	0.5	5.6	2.5	5.6	0.5	1.8	0.7	1.0	3.0	0.5	1.0	9.8	1.8	1.4	3.0	4.1	1.4	0.3	0.7	1.1		2:45	12	5	3	0	60	85	
7	11	M	12.0	0.0		6.7	0.3		8.0	0.5	2.5	0.8	0.5	4.6	1.4	4.9	3.6	0.4	0.0	0.0	0.4	1.0		2:43	12	4	2	2	67	88	
8	11	M	0.5	4.0	4.4	0.0	4.0	3.7	0.4	4.5	0.8	0.6	1.0	0.0	2.4	1.7	1.4	2.2	3.6	0.0	0.0		2:58	11	7	2	0	55	90		
9	11	F	1.9	1.3	0.4	0.5	0.0	3.5	6.0	0.0	0.5	0.0	1.2	1.9	1.4	8.8	1.8	1.0	1.0	1.0	0.2	0.0		2:21	15	1	2	2	83	88	
10	11	M	3.0	2.6	0.5	1.6	0.0	2.0	8.0	0.6	5.9	0.5	0.0	1.0	0.4	6.0	1.0	0.0	0.9	1.8	0.5	0.8		3:28	16	1	3	0	80	85	
11	11	F	4.7	0.5	0.0	1.8	0.6	2.6	2.6	1.4	0.1	1.4	0.0	4.0	5.2	1.4	0.0	0.0	1.8	1.9	1.0	0.9		2:36	15	4	1	0	75	95	
12	12	F	4.0	0.0	0.7	4.0	1.0	3.9	0.4	0.0	2.4	0.3	0.4	0.0	0.0	0.0	2.2	0.5	4.0	3.2	0.7	0.5		3:08	13	7	0	0	65	100	
13	13	M	3.7	2.8	0.2	2.6	0.0	1.5	5.6	0.2	3.2	0.0	1.8	3.2	0.0	0.6	0.2	0.8	0.0	4.6	0.0	0.0		3:28	13	6	1	0	65	95	
14	13	F	1.5	3.0			0.0	7.9		0.2	1.6				0.6		0.6	1.5	1.6	0.8				2:38	8	2	1	9	72	90	
15	13	F	2.6	0.4		6.9	0.4	0.5	0.0	0.0	2.9	1.6	0.0	3.0	1.8	1.4	1.8	0.0	0.8	1.8	1.4	1.0		2:27	16	2	1	1	84	94	
16	13	M	4.0	0.5		1.8	0.2	0.0		2.1	3.1			3.6											2:18	4	4	0	12	67	100
17	14	M	7.2	0.4	1.3	1.0	0.4	2.7	0.4	2.3	0.0	0.0	1.0	3.8	1.2	2.2	0.0	0.4	0.5	1.2	1.9	0.4		3:12	14	4	2	0	70	90	
18	14	F	1.2	1.8	6.0		0.0		0.4	6.9			0.5												2:58	5	0	2	13	71	71
19	14	F					0.2			0.8			2.6						0.0	0.6	0.4				2:38	4	1	0	15	80	100
20	14	M	1.3	10.0	2.9	2.4	1.0	0.0	0.5	0.8	1.5	0.0		1.6	0.8	0.0	0.0	0.0	4.6	0.0	0.0	1.0		3:41	15	3	1	1	79	94	
21	14	M	0.0	0.0	2.2		0.0																		2:21	3	0	1	16	75	75
22	14	F	1.6	0.0	1.0	1.8		0.0	0.8	0.8	1.6	0.0	0.0	4.5	0.4	4.4	1.0	1.6	0.0	2.4	0.0	0.0		3:17	16	2	0	1	84	94	
23	14	M	2.4	0.0	1.6	1.8	0.0	1.2	2.5	0.4	0.4	0.0	0.0	5.8	0.6	0.5	1.5	1.3	0.5	1.8	0.0	0.0		3:05	17	2	1	0	85	95	
24	14	M	0.4	0.0	1.6	2.1	0.0	0.8	6.6	0.0	1.6	0.0	0.4	5.2	0.5	0.5	1.0	0.8	0.8	1.9	0.0	0.0		3:53	17	1	2	0	85	90	
25	15	F	0.4	0.9	1.0	0.0	10.0	0.0	1.0	0.8	1.2	0.8	1.0	4.7	0.5	1.6	0.0	1.0	0.4	1.6	0.0			2:39	17	1	1	1	89	94	
26	15	M	5.9	1.3	0.0	0.4	0.6	0.0	3.1	1.9	0.0	0.4	0.0	4.8	1.3	3.2	0.8	1.9	3.0	2.5	0.0	1.0		3:56	13	5	2	0	65	90	
27	16	M	3.4	0.6	0.9	1.2	1.0	0.0	0.5	0.0	0.8		1.4	1.6	0.6	0.9	1.0	0.0	0.5	2.5	1.0	1.0		4:05	17	2	0	1	89	100	
28	16	M			0.0			0.0		0.9	0.4	0.5		0.8	1.0	0.9	1.4	0.0	1.5	1.2	0.9			2:27	13	0	0	7	100	100	
29	16	F	1.9	0.0	1.2	1.0	0.0	0.4	0.5	0.8	2.0	0.6	0.9	4.7	1.2	0.9	0.5	1.0	3.2	1.2	0.0	1.0		3:59	18	2	0	0	90	100	
30	16	M	0.0	0.0	0.5	4.9	26.0	0.0	0.5	0.0	1.6	0.0	0.0	0.8	8.1	0.0	5.0	0.5	4.6	2.7	0.0	1.6		3:45	14	4	2	0	70	90	
31	16	F	2.9	0.0	0.8	0.5	0.0	2.3	9.0	1.0	9.9	0.5	1.0	1.4	0.8	3.2	6.4	1.2	0.5	0.0	0.0	0.0		4:50	14	3	3	0	70	85	
32	16	F	0.6	0.0	2.5	0.0	0.0	5.4	0.4	0.0	0.0	0.0	0.3	2.4	1.0	0.9	0.4	1.0	0.0	0.0	9.4	0.0		3:24	16	2	2	0	80	90	
33	16	M	0.8	1.5	0.0	1.8	0.0	5.8	2.5	0.4	0.4	0.0	0.0	3.6	8.0	1.3	0.0	0.5	0.6	0.8	0.9	1.4		3:34	16	2	2	0	80	90	
34	16	M	0.4	0.0	0.0	1.6	0.0	0.4	1.8	0.8	0.0	0.0	0.0	0.0	3.5	0.8	0.5	0.8	0.0	0.5	0.8	0.4		3:51	19	1	0	0	95	100	
35	17	F	0.9	0.0		3.9	0.0	1.6	0.0	2.2	0.0	0.0	0.5	7.8	1.6	2.0	0.0	0.0	1.0	1.2	0.0	0.0		3:28	16	2	0	1	84	100	
36	17	F	6.5	0.3	0.0	0.0	1.0	0.8	9.0	0.0	0.4	0.0	1.0	3.2	0.4	0.0	0.5	0.4	0.4	0.8	1.3	0.0		4:00	16	2	2	0	80	90	
37	17	M	0.4	0.0	0.0	3.3	0.4	1.5	8.0	0.0	0.4	0.4	0.0	3.1	0.0	4.2	7.1	0.0	0.6	0.0	0.0	0.0		4:31	15	3	2	0	75	90	
38	18	M	1.5	0.5			1.7	0.0	0.0	0.5	1.6	0.0	1.3	0.8	1.6	0.0	0.4	1.4	0.6	2.1	1.8	0.0		3:46	16	1	1	2	89	94	
39	18	M	1.9	0.7	1.6	0.0	0.0	0.0	8.5	0.8	0.0	0.8	1.9	1.4	0.5	5.2	1.0	5.7	5.7	0.0	1.2	0.0		3:26	15	0	5	0	75	75	
40	38	F	1.6	2.9	0.0	1.9	0.0	0.9	0.4	0.5	0.0	0.0	0.0	2.4	0.6	2.1	1.5	1.2	1.2	0.0	1.3	0.0		4:29	16	3	1	0	80	95	

number of landmarks located within the ranges, 0 - 2mm, 2 - 5mm, greater than 5mm and the number of points not within the search window. The number of points in these ranges is also expressed as a percentage of the landmarks whose positions fell within the search window.

**4. Discussion**

The categorized summary in Table 6.2 has been plotted in Fig. 6.3. Since training is performed after each x-ray is processed, the plot shows the performance trend with training. The white area represents those points which were located within 2mm of the target. The light grey area represents the portion of points located between 2 and 5mm from the target. The dark grey is proportional to the number of points whose located position was greater than 5mm in error. The black area represents

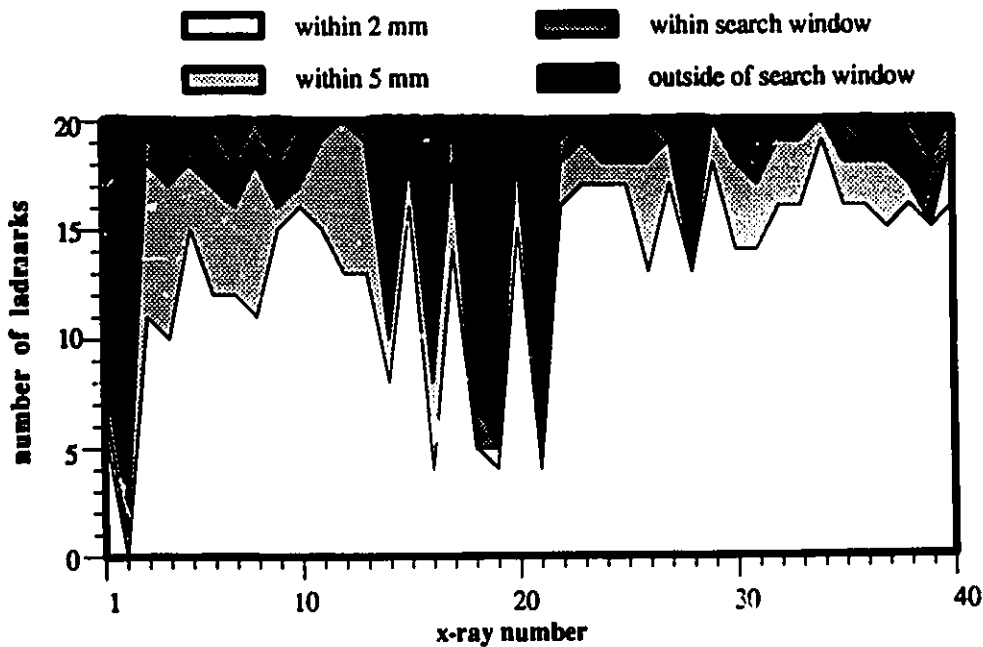


Fig. 6.3. Plot of number of landmarks located within an error of (i) 2mm, (ii) 5mm and (iii) were within the search window.

those points which could not be found because they were not within the search window.

A noticeable trend is observed as a decrease in black area with time. This is attributed to the search window training. As the search windows are shifted and adjusted, the frequency of misses decreases. The spikes near the 20th x-ray occur because the search windows are allowed to shrink. After a miss of this type occurs, the training immediately enlarges the search window to encompass that possible position in future searches.

It would be unfair to assess the shape recognition algorithm from the plot of Fig. 6.3 which includes points that were not within the search window. In Fig. 6.4 the data has been plotted as a percentage of those points which were within the search windows. The performance trend of

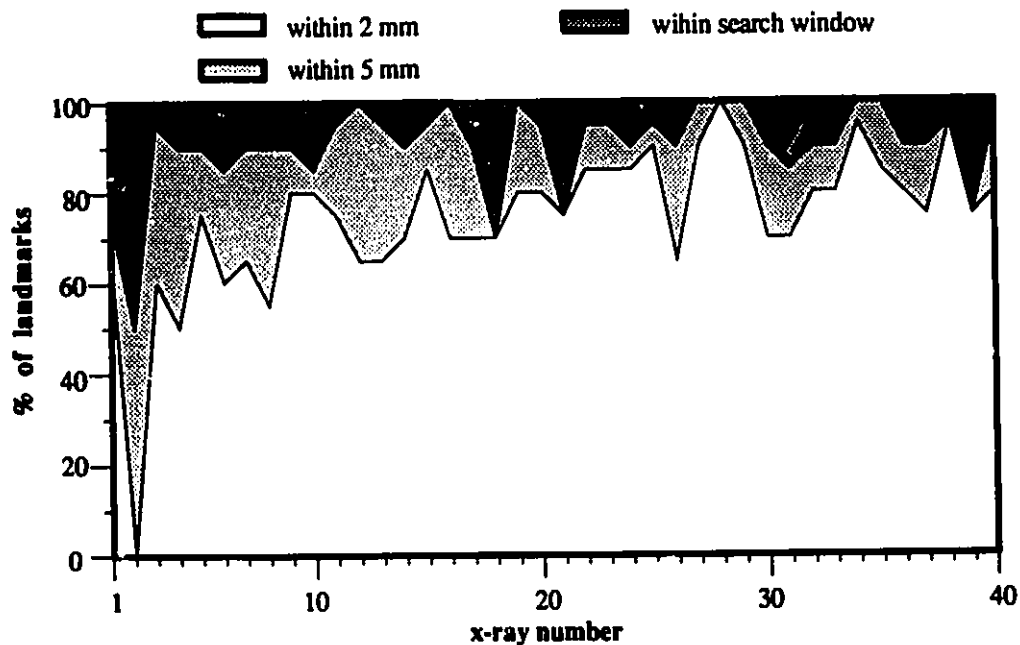


Fig. 6.4. Plot of number of landmarks located to within an error of (i) 2mm, (ii) 5mm, and (iii) further than 5mm, as a % of those points which were within the search window.

the algorithm becomes clearly visible in this plot. The number of landmarks located to within 2mm of the actual position, the white area, steadily increases from 60% at the start of training to a level of approximately 85% after 40 x-rays. The number of landmarks located between 2 and 5mm from the actual position, the light grey area, steadily decreases from about 30% to nearly 5%. The number of landmarks which were in error by greater than 5mm remained unchanged at approximately 10% throughout the training. This persistent problem with 10% of the landmarks might be explained by analyzing the results on a landmark categorized basis.

The bar graph of Fig. 6.5 summarizes the search results from the 40 x-rays for each landmark. The figure provides an assessment of the target recognition algorithm for each landmark. It is obvious from the figure that the anterior point of the occlusal plane accounts for most of the misses. Examining the shape of this landmark on several x-rays reveals a widely varying set of possibilities. Anything from an overbite of 20mm to an underbite is possible. The algorithm could not be expected to recognize this wide range of possible shapes using a single model. Similar problems exist with other landmarks surrounding the teeth. Because the teeth move, grow in at a variety of angles, and are sometimes missing, landmarks involving teeth may take on a variety of shapes. Such a variety of possible shapes may not be representable using a single model.

A different problem occurs with the landmark orbitale. This landmark has a number of location errors between 2 and 5mm. The problem may be attributed to the size or scale of this landmark. The landmark is located at the base of the large subtle curve outlining the eye socket. At the scale of the small  $20 \times 20$  structuring elements the landmark is obscure and not noticeable. It is only by stepping back and viewing the

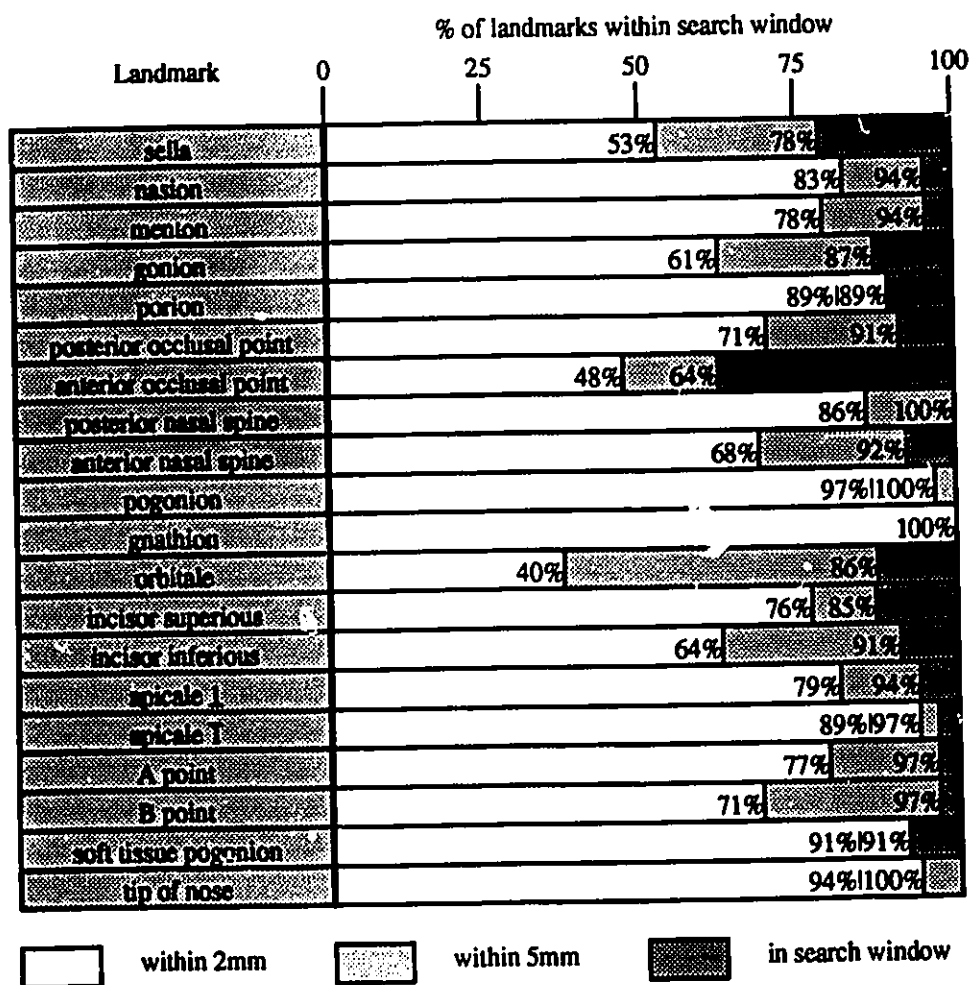


Fig. 6.5. Summarized results per landmark. Number of times located to within an error of (i) 2mm, (ii) 5mm, and (iii) further than 5mm, as a % of those which were within the search window.

landmark at a larger scale that it becomes clear. This suggests that too much resolution is being used to locate the landmark and thus, rather than converging on the landmark the algorithm is converging on some smaller shape or shapes within the landmark.

The time to locate the 20 landmarks on 40 x-rays using an IBM-AT running at 8MHz has been plotted in Fig. 6.6. The jagged nature of this plot reflects the algorithm's ability to adjust to x-rays of varying sizes.



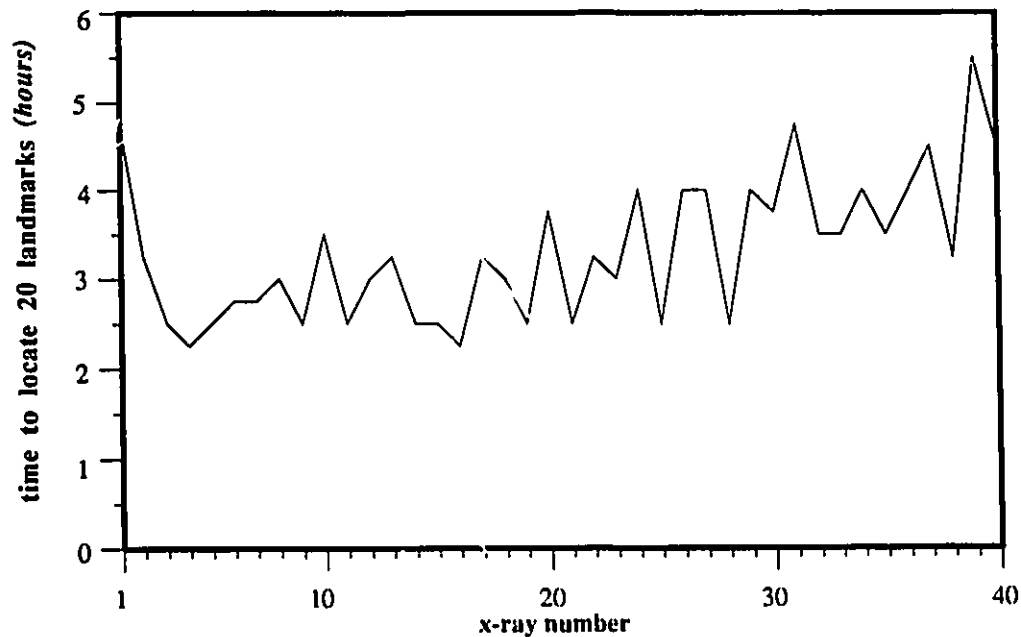


Fig. 6.6. Plot of the time required to locate 20 landmarks over 40 x-rays.

The initial dip followed by a gradual increase in processing time coincides with increases and decreases in search window sizes during training. Overall, the system is settling at a processing time of approximately 4 hours and 30 minutes. Although a processing time of this magnitude is unacceptable for a cephalometric work station, presently available 386 based machines running at 33MHz run nearly 8 times faster and would cut the processing times to approximately 30 minutes. This is still not within the suggested 10 minute processing time, but it would not be unreasonable to expect that a sufficiently powerful affordable machine will become available before too long. The processing time for locating more than 20 landmarks would not increase dramatically. Most of the time is spent locating the first few points which require large search windows.

Subsequent landmark locations become more predictable and thus require smaller search windows.

## ***B. Experiment 2 — Locating after training***

### ***1. Purpose***

The purpose of this experiment is to assess the after training long term performance of the shape recognition algorithm.

### ***2. Procedure***

The system is trained to locate 20 landmarks using 40 x-rays. The shape recognition algorithm is then applied to locate the landmarks on the same 40 x-rays used during training. The theory behind this is that with training the algorithm will eventually be exposed to most of the possible shape variations of each landmark. Therefore, processing x-rays which were previously used for training should simulate the long term state of this system. Each x-ray is processed and the landmark positions determined by the algorithm are compared to those determined by the operator. The difference in mm between the respective positions is recorded as the landmark's location error.

### ***3. Observations***

Location errors for the 20 landmarks on each x-ray are collected in Table 6.3. The table also contains a categorized summary of the number and percentage of points being located within (i) 2mm, (ii) 5mm, and (iii) within the search windows.

### ***4. Discussion***

On average the number of landmarks located within 2mm was 88%. This is not far from the 85% predicted in experiment 1. The number of landmarks located between 2 and 5mm remained near 5% while the

**TABLE 6.3.**  
**LOCATION ERRORS FOR EXPERIMENT #2 (mm)**

x-ray			landmark																time	summary				% of points in search window					
No.	Age	Sex	Se	Na	Me	Go	Po	POcc	AOcc	PNS	ANS	Fog	Gn	Or	Is I	Is I	Ap I	Ap I		A point	B point	Soft Fog	Tip of Nose	points < 2mm	points 2 - 5 mm	points > 5mm	not in window	% < 2mm	% 2 - 5mm
1	9	F	-	-	0.0	0.8	0.0	1.2	0.0	0.4	1.6	0.0	0.6	0.5	1.0	1.2	3.1	1.2	1.2	1.6	0.0	0.5	3:51	17	1	0	2	94	100
2	10	F	1.6	1.0	1.2	1.6	0.0	0.4	1.0	1.8	4.4	0.0	0.0	2.4	1.8	1.9	1.4	1.0	1.4	0.5	0.5	1.0	4:28	17	2	1	0	85	95
3	10	F	1.6	0.5	0.0	0.9	0.0	0.0	0.0	0.0	1.0	0.0	0.0	0.4	0.0	0.4	5.9	0.0	0.5	0.0	0.0	0.0	4:26	17	0	3	0	85	85
4	10	F	3.6	0.6	0.0	0.6	0.5	1.2	0.0	0.0	0.4	3.6	0.0	0.9	1.0	0.5	3.6	0.9	0.8	0.8	0.0	0.0	4:23	16	3	1	0	80	95
5	11	M	1.4	3.1	1.0	0.0	0.0	0.8	0.0	0.0	0.0	0.0	0.0	0.0	1.9	0.0	3.5	0.8	1.4	1.6	0.0	0.0	4:42	18	2	0	0	90	100
6	11	F	0.5	0.6	0.6	0.5	0.0	0.9	0.5	0.0	0.8	0.8	0.0	2.3	1.0	0.4	0.8	1.0	0.4	0.0	0.8	0.5	5:02	19	1	0	0	95	100
7	11	M	1.6	0.9	0.8	0.0	0.0	2.9	8.2	0.4	1.9	0.6	1.0	0.4	0.8	5.9	2.4	0.0	4.3	1.4	0.0	0.4	4:28	15	3	2	0	75	90
8	11	M	1.9	1.2	1.0	1.0	0.0	0.8	8.5	0.8	0.0	0.0	1.2	1.2	0.9	8.2	1.2	0.0	1.5	0.0	0.0	0.0	4:57	17	0	3	0	85	85
9	11	F	2.0	0.0	1.2	0.0	0.0	1.2	9.6	1.0	0.4	0.5	0.6	1.6	0.5	1.2	1.9	1.0	0.9	0.6	0.4	0.0	4:10	19	0	1	0	95	95
10	11	M	0.0	1.6	0.5	0.8	0.0	0.0	9.1	0.8	8.4	1.8	1.2	1.2	0.0	8.4	0.6	0.0	1.0	0.5	0.8	0.0	5:30	17	0	3	0	85	85
11	11	F	2.5	2.0	0.8	0.4	0.0	1.2	11.0	0.0	-	0.5	0.4	1.8	1.4	5.0	0.0	1.3	1.0	0.4	0.0	0.0	4:24	14	3	2	1	74	89
12	12	F	1.4	0.9	1.0	0.5	0.0	0.0	0.5	0.0	0.0	0.0	1.2	0.4	0.0	0.6	1.5	1.6	0.0	1.0	0.0	0.0	4:28	20	0	0	0	100	100
13	13	M	0.5	2.7	1.2	0.0	0.0	0.4	9.1	0.0	1.9	0.0	0.0	1.6	1.2	4.5	0.0	1.0	2.8	0.0	0.0	0.0	5:15	16	3	1	0	80	95
14	13	F	1.6	0.4	0.0	0.0	0.0	6.6	0.0	0.8	0.0	0.0	0.0	1.8	1.0	0.0	0.8	1.0	1.0	0.5	0.0	0.9	5:07	18	0	2	0	90	90
15	13	F	0.0	0.0	1.9	0.0	0.0	0.4	0.0	0.0	0.0	0.8	0.6	1.6	0.0	0.0	0.0	0.0	0.0	4.3	0.0	0.0	3:53	19	1	0	0	95	100
16	13	M	2.4	0.0	1.0	0.0	0.0	11.0	0.0	0.0	0.0	0.0	1.9	-	-	0.0	1.6	0.0	0.0	0.0	0.0	0.0	4:13	16	1	1	2	80	89
17	14	M	5.4	0.0	1.2	0.4	0.0	0.0	9.6	0.4	8.5	0.0	1.0	0.0	0.9	1.2	0.5	1.0	1.0	0.0	0.0	0.0	4:49	17	0	3	0	85	85
18	14	F	0.0	0.0	1.0	1.2	0.0	0.8	9.2	0.0	1.9	0.0	0.0	0.0	0.5	1.8	4.2	0.0	7.6	0.0	0.0	0.0	5:27	16	1	3	0	80	85
19	14	F	-	0.0	0.0	0.0	0.8	1.6	1.0	0.4	0.0	0.0	0.0	2.4	0.5	4.5	0.0	0.0	1.4	0.0	0.0	0.0	5:03	16	2	1	1	84	95
20	14	M	0.0	0.8	-	0.4	0.0	1.6	0.0	0.0	1.2	2.7	-	0.4	1.0	0.4	0.0	0.8	4.5	0.0	0.0	0.0	4:30	16	2	0	2	89	100
21	14	M	0.0	1.8	1.2	0.8	0.8	0.6	0.0	0.8	0.8	0.8	1.2	0.0	4.8	0.8	1.0	1.0	0.0	0.0	0.0	0.0	5:35	19	1	0	0	95	100
22	14	F	2.0	1.2	0.0	0.6	0.0	0.4	0.0	0.0	0.4	0.5	1.0	1.4	0.0	0.8	0.0	0.0	0.0	0.0	0.0	0.0	5:05	20	0	0	0	100	100
23	14	M	1.9	0.0	1.2	0.0	0.0	6.8	1.5	0.9	0.8	0.0	0.0	1.4	0.9	0.8	0.9	0.5	0.8	0.5	0.4	0.0	4:46	20	0	0	0	100	100
24	14	M	0.0	0.6	0.0	0.0	0.0	0.8	7.1	0.0	0.0	0.0	0.0	1.9	0.4	0.5	0.0	0.0	0.5	0.0	0.0	0.0	5:35	19	0	1	0	95	95
25	15	F	1.2	1.0	0.0	0.0	0.0	0.0	0.0	0.0	0.4	0.0	0.0	0.0	0.5	1.4	0.0	1.0	0.0	0.0	0.0	0.0	4:09	20	0	0	0	100	100
26	15	M	1.9	0.0	0.4	1.0	0.5	0.4	0.0	0.8	0.0	1.3	0.0	0.0	1.4	5.9	1.2	0.0	6.7	1.3	0.0	0.0	5:32	17	0	3	0	85	85
27	16	M	4.2	0.0	0.8	0.0	0.8	0.0	0.0	0.0	0.0	0.0	-	-	1.0	0.5	4.7	0.0	0.0	1.4	0.5	0.0	5:36	16	2	0	2	89	100
28	16	M	1.3	1.8	1.0	1.2	0.0	0.8	0.0	0.8	0.0	0.0	0.0	0.8	0.0	0.0	0.0	7.0	0.5	0.0	0.0	0.0	4:21	19	0	1	0	95	95
29	16	F	3.8	0.0	0.6	0.6	0.0	0.4	0.6	0.0	0.0	0.8	0.0	0.0	1.2	0.0	0.0	0.0	4.3	0.0	0.0	0.0	4:48	18	2	0	0	90	100
30	16	M	0.0	0.8	0.0	0.0	2.2	0.0	0.0	0.8	0.8	0.0	0.0	1.9	8.5	0.0	4.8	0.0	3.2	0.0	0.0	0.0	4:13	16	2	2	0	80	90
31	16	F	2.9	0.0	1.8	0.0	1.3	1.6	11.0	1.0	1.2	0.0	1.2	0.0	0.8	2.2	1.8	0.0	2.5	0.0	0.0	0.0	5:43	16	3	1	0	80	95
32	16	F	0.0	0.0	3.7	0.0	0.0	7.4	0.8	0.0	0.0	0.0	0.0	0.0	0.6	1.5	1.3	0.0	1.5	0.0	0.0	0.0	4:18	18	1	1	0	90	95
33	16	M	0.6	1.8	1.0	0.8	0.0	5.8	5.8	0.0	0.0	0.0	0.0	1.6	5.8	4.8	1.2	0.0	0.5	0.0	0.0	0.0	4:27	16	1	3	0	80	85
34	16	M	0.0	0.0	0.0	1.5	0.0	0.0	1.9	0.0	0.0	0.0	0.0	2.9	3.1	1.6	1.9	0.0	1.0	0.0	0.0	0.0	4:47	18	2	0	0	90	100
35	17	F	0.0	0.0	0.0	0.0	0.0	1.8	1.2	1.8	0.0	0.0	0.0	0.0	1.5	0.4	1.6	0.0	1.0	0.0	0.0	0.0	3:52	20	0	0	0	100	100
36	17	F	6.3	0.5	0.0	0.0	0.0	1.2	0.0	0.0	0.0	0.0	0.0	0.0	0.0	0.0	0.0	0.0	0.0	0.0	0.0	0.0	4:34	19	0	1	0	95	95
37	17	M	1.3	1.2	0.0	0.0	0.0	1.8	11.0	0.0	0.0	1.2	0.0	1.0	1.2	1.2	5.8	0.0	0.5	1.6	0.0	0.0	5:22	17	0	3	0	85	85
38	18	M	0.0	0.0	2.0	0.0	0.0	0.0	0.0	0.0	0.4	0.0	2.1	0.0	1.0	1.9	0.5	0.0	1.5	2.4	0.0	0.0	4:20	17	2	1	0	85	95
39	18	M	0.0	0.0	1.2	0.0	0.0	0.8	5.4	0.0	0.8	1.2	2.7	0.0	0.0	5.5	4.7	3.0	0.0	0.0	0.0	0.0	5:25	15	3	2	0	75	90
40	39	F	0.0	1.8	0.0	0.0	0.0	1.2	0.8	0.0	0.0	0.0	0.0	0.0	0.8	1.8	0.8	1.0	0.9	0.0	1.2	0.0	0.0						

number of landmarks missed by more than 5mm dropped slightly to 7%. The processing time remained at roughly 4 hours and 30 minutes.

Analyzing the results for individual landmarks reinforces the discussion from experiment 1. The percentage of times a landmark was located within (i) 2mm, (ii) 5mm and (iii) the search window is illustrated in the bar graph of Fig. 6.7. Notice again that the landmarks causing the

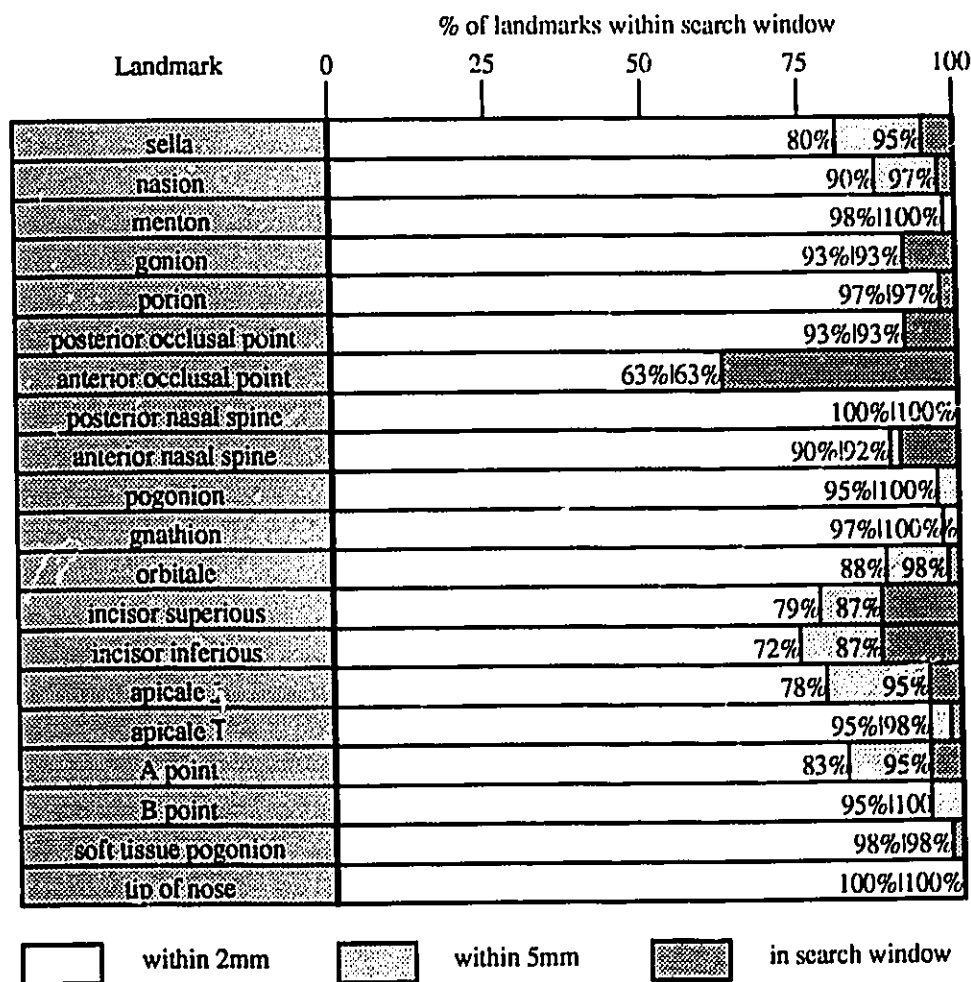


Fig. 6.7. Summarized results per landmark. Number of times located to within an error of, (i) 2mm, (ii) 5mm and, (iii) further than 5mm, as a % of those which were within the search window.

greatest difficulty are those involving the incisors. Actually, the anterior occlusal point, incisor superious, and incisor inferious account for 54% of times in which a landmark could not be located to within 5mm.

The results have also been statistically summarized in Table 6.4. The overall mean error in the locations of the landmarks is 1.1mm with a standard deviation of 1.9mm. Again, most of this error is attributed to the incisional landmarks. Notice also that the standard deviations are sometimes as much as 3 times the mean. Scanning the data in Table 6.3 reveals that misses, although rare, have a substantial error when they occur.

**TABLE 6.4.**  
**STATISTICAL SUMMARY OF LOCATION ERRORS IN EXPERIMENT #2**

Landmark	location error (mm)	
	Mean	Standard Deviation
sella	1.4	1.5
nasion	0.9	1.4
menton	1.2	3.2
gonion	1.2	3.5
porion	0.6	3.4
posterior occlusal point	1.1	1.6
anterior occlusal point	3.5	4.4
posterior nasal spine	0.3	0.4
anterior nasal spine	1.1	2.4
pogonion	0.4	0.7
gnathion	0.4	0.6
orbitale	1.1	1.7
incisor superious	2.4	3.8
incisor inferious	2.1	2.3
apicale 1	1.4	1.7
apicale $\bar{1}$	0.6	1.2
A point	1.4	1.7
B point	0.5	0.9
soft pogonion	0.3	1.8
tip of nose	0.08	0.2
average	1.1	1.9

## VII. RECOMMENDATIONS FOR FUTURE WORK

The experiments showed that on average, 88% of the landmarks will be located to within 2mm of their verified positions. Position errors less than approximately 2mm do not significantly affect the cephalometric measurements and are thus satisfactory. On the other hand, errors exceeding this amount influence the measurements beyond an acceptable amount. Operator intervention is then required to adjust the positions of the landmarks in error. For a shape recognition algorithm operating on such diverse shapes and inconsistent x-ray images, 88% is very good. Yet, for an automatic cephalometric evaluation system, it falls short. What is required is 100% recognition, most of the time. Only with such a performance level would this algorithm be viable and useful for automatic landmarking of cephalograms. An automatic system requiring frequent operator intervention would obviously be impractical. Further work is necessary to achieve this desired level of performance. The following recommendations come from experimental observations and recognized limitations imposed by this implementation of the algorithm.

### *A. Multiple Models per Landmark*

One of the first observations made in the experiments was that most of the problems were caused by only a few landmarks. In particular, the landmarks involving the incisors, such as the anterior occlusal point, incisor superious and incisor inferious accounted for 54% of the landmarks located beyond the acceptable 2mm. A quick glance at some x-rays reveals

the wide range of possible forms that these landmarks can assume. The actual shapes of the incisors remain unchanged from x-ray to x-ray but, their angle of protrusion and their positions about one another varies drastically. Anywhere from an overbite of 20mm, to an underbite is observed.

Representing such a wide range of possibilities with one set of structuring elements, or one view, is unreasonable. What is required is a family of views or shapes that represent the possible forms that a landmark may assume. A similar suggestion was provided by Crimmons and Brown [17] with equation (4.3) in reference to general shape recognition. This idea may be applied to the grey-level shape recognition algorithm developed in this work.

The application permitted the assumption that one landmark was always present in the search space. Consequently, the most likely position of a landmark is determined by finding the minimum in the shape recognition error function. If separate versions of the landmark's defining structuring elements produce separate shape recognition error functions, then it should be expected that the version which most closely matches the landmark's appearance in the image will produce the strongest minimum. If  $D_\gamma$  defines the shape recognition error functions where  $\gamma \in \Gamma$  is the family of variations of the landmark, then the landmark is found where the strongest minimum occurs or where

$$\min_{\gamma \in \Gamma} [ \min_{x,y} D_\gamma(x,y) ] . \quad (7.1)$$

### ***B. Variable Sized Structuring Elements***

This recommendation comes both from observed problems and from limitations imposed by this implementation. In the experiments, structuring elements were all assigned a fixed size of  $20 \times 20$  pixels. This restriction



causes problems for landmarks neighboring other unrelated features. For example, in Fig. 7.1 the lips which are near the tips of the incisors interfere with the appearance of these landmarks. If variable sized structuring elements were used perhaps this type of interference could have been avoided.

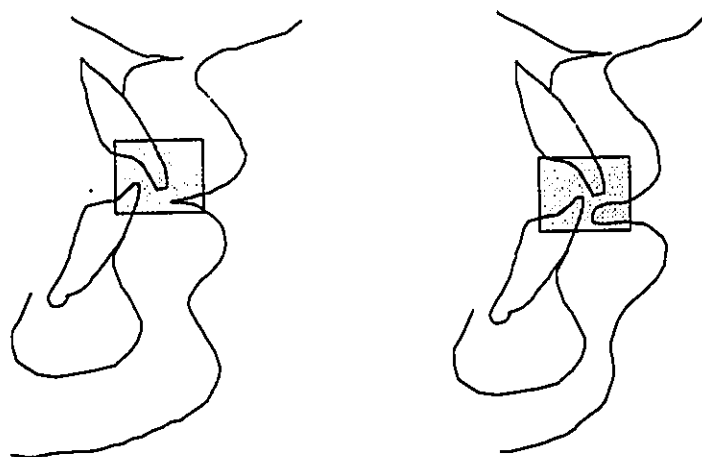


Fig. 7.1. An example of the possible unwanted interference caused by the lips on the structuring element defining the tip of the incisors.

One method of determining the best size for a structuring element may be implemented through the training algorithm. In addition to calculating the cumulative average of each pixel in a structuring element, their variance may also be calculated. A flexible-sized structuring element may then be achieved by using only those pixels with a variance below some selected threshold value. In this manner the pixels or regions in the structuring element which are found to vary unacceptably can be excluded from the search.

### ***C. Variable Resolution Structuring Elements***

On another front, the  $20 \times 20$  size was too small for the landmark orbitale. This landmark, appears at the base of a large subtle curve on the x-ray. The landmark is clearly visible from a distance, but attempting to find this landmark through a  $20 \times 20$  window is difficult. The large gradual feature is easily obscured by smaller features which predominate in the relatively small structuring element window. The  $20 \times 20$  pixels is sufficient but the scale or resolution to which they have been applied is inappropriate. Permitting structuring elements to be defined at various resolutions would add flexibility to the implementation of the shape recognition algorithm.

### ***D. Search Window Shapes***

One final recommendation concerns the search windows. The sizes of these windows could be optimized further by adding some complexity to their shape. In this work the simplest form, a centred rectangle, was used. Shifting the centre alone would reduce the required window sizes. Whenever a landmark's position forced an enlargement of one side of a trained search window, the enlargement was done symmetrically to both sides. This could have been avoided by using a more complex definition for the window size. For example, rather than specifying a height and width for the window, separate heights for the top and bottom halves and separate widths for the left and right sides of the window could have been used. The idea could be carried further to incorporate different window shapes.

## VIII. CONCLUSIONS

### *A. Contribution*

A new automatic shape recognition algorithm based on grey-scale mathematical morphology was developed to extract craniofacial landmarks from cephalograms. The morphological shape recognition algorithm of Crimmins and Brown [17] was modified so that the search for a grey-level target becomes a search for minima in the shape recognition error function computed using max-min operations. It was then found that by replacing the max-min operation with the statistical standard deviation, the algorithm became less susceptible to noise and more accommodating to subtle differences in skeletal topographies. Decomposition was used to desensitize the algorithm to size differences. A new technique was also devised for minimizing the search window sizes, thus improving speed and minimizing the detection of false targets.

### *B. Summary of Results*

The algorithms were implemented in a cephalometric work station on an IBM-AT running at 8MHz. The system was trained to locate 20 landmarks. Tests were performed using 40 x-rays from male and female patients ranging from 9 to 39 years of age. Two separate experiments were conducted to determine; (i) the progress with training and (ii) the long term performance of this system.

In the first experiment, the number of landmarks located to within 2mm increased steadily from 60% to 85% on average after 40 x-rays. The processing time settled to approximately 4 hours and 30 minutes.

In the second experiment, the number of landmarks located within 2mm was 88% on average. The overall mean error in the located positions of the landmarks was 1.1mm with a standard deviation of 1.9mm. Approximately 50% of the position errors greater than 2mm were due to the incisional landmarks. It was discovered that these landmarks take on a variety of forms and could not be adequately represented by a single set of structuring elements.

## IX. REFERENCES

- [1] T. Rakosi, *An Atlas and Manual of Cephalometric Radiography*, London: Wolfe Medical Publications, 1982.
- [2] A. D. Lévy-Mandel, A. N. Venetsanopoulos, and J. K. Tsotsos, "Knowledge-Based Landmarking of Cephalograms," *Computers and Biomedical Research*, vol. 19, pp. 282-309, 1986.
- [3] L. Mero and Z. Vassy, "A Simplified and Fast Version of the Hueckel Operator for Finding Optimal Edges in Pictures," *In Proceedings of the 4th International Joint Conference on Artificial Intelligence*, Tbilissi, Georgia, USSR, Sept. 1975, pp. 650-655.
- [4] S. T. Nugent, S. Parthasarathy, P. H. Gregson and D. F. Fay, "Feature Recognition in Skull X-Rays Using Digital Image Processing Techniques," *in Proceedings of the 25th International ISA Biomedical Sciences Instrumentation Symposium*, Colorado Springs, CO, Apr. 25-26, 1988, pp. 5-7.
- [5] S. Parthasarathy, S. T. Nugent, P. H. Gregson and D. F. Fay, "Automatic Landmarking of Cephalograms," *Computers and Biomedical Research*, vol. 22, pp. 248-269, 1989.
- [6] J. L. Contreras-Vidal and J. Garza-Garza, "A Knowledge-Based System for Image Processing and Interpretation of Cephalograms," *In Proceedings of the Canadian Conference on Electrical and Computer Engineering*, Ottawa, ONT, Sept. 4-6, 1990, pp. 75.1.1-75.1.4.
- [7] P. H. Jackson, G. C. Dickson, and D. J. Birnie, "Digital Image Processing of Cephalometric Radiographs: A Preliminary Report," *British Journal of Orthodontics*, vol. 12, pp. 122-132, 1985.

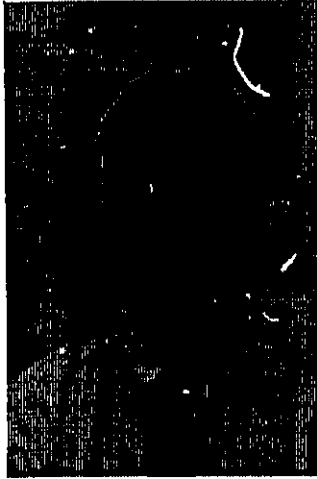
- [8] A. M. Cohen and A. D. Linney, "A low Cost System for Computer-Based Cephalometric Analysis," *British Journal of Orthodontics*, vol. 13, pp.105-108, 1986.
- [9] A. M. Cohen, H. H-S. Ip, and A. D. Linney, "A Preliminary Study of Computer Recognition and Identification of Skeletal Landmarks as a New Method of Cephalometric Analysis," *British Journal of Orthodontics*, vol. 11, pp. 143-154, 1984.
- [10] A. Rosenfeld and A. C. Kak, *Digital Picture Processing*, New York: Academic Press, 1982.
- [11] R. O. Duda and P. E. Hart, *Pattern Classification and Scene Analysis*, New York: Wiley, 1973.
- [12] R. Y. Wong and E. L. Hall, "Performance Comparison of Scene Matching Techniques," *IEEE Transactions on Pattern Analysis and Machine Intelligence*, vol. PAMI-1, no. 3, pp. 325-330, July 1979.
- [13] K. E. Price, "Relaxation Matching Techniques—A Comparison," *IEEE Transactions on Pattern Analysis and Machine Intelligence*, vol. PAMI-7, no. 5, pp. 617-623, Sept. 1985.
- [14] T. M. Cover and P. E. Hart, "Nearest Neighbor Pattern Classification," *IEEE Transactions on Information Theory*, vol. IT-13, pp. 21-27, Jan. 1967.
- [15] C. H. Chen, "A Theory of Bayesian Learning Systems," *IEEE Transactions on Systems Science and Cybernetics*, vol. SSC-5, no. 1, Jan. 1969.
- [16] M. W. Roth, "Survey of Neural Network Technology for Automatic Target Recognition," *IEEE Transactions on Neural Networks*, vol. 1, no. 1, March 1990.
- [17] T. R. Crimmins and W.M. Brown, "Image Algebra and Automatic Shape Recognition," *IEEE Transactions on Aerospace and Electronic Systems*, vol. AES-21, no. 1, pp. 60-69, Jan. 1985

- [18] L. G. Shapiro, R. S. MacDonald and S. R. Sternberg, "Shape Recognition with Mathematical Morphology," in *Proceedings of the 8th International Conference on Pattern Recognition*, Paris, France, Oct. 27-31, 1986, pp.416-418.
- [19] F. Y. Shih and O. R. Mitchell, "Automated Fast Recognition and Location of Arbitrarily Shaped Objects by Image Morphology," in *Proceedings of the Computer Society Conference on Computer Vision and Pattern Recognition*, Ann Arbor, MI, June 5-9, 1988, pp. 774-779.
- [20] P. Maragos, "Optimal Morphological Approaches to Image Matching and Object Detection," in *Proceedings of the Computer Society Conference on Computer Vision and Pattern Recognition*, Ann Arbor, MI, June 5-9, 1988, pp. 695-699.
- [21] R. E. Moyers, *Handbook of Orthodontics*, 4th Ed., Chicago: Yearbook Medical Publishers, 1988.
- [22] G. Matheron, *Random Sets and Integral Geometry*, New York: Wiley, 1975.
- [23] J. Serra, *Image Analysis and Mathematical Morphology*, London: Academic Press, 1982.
- [24] H. J. A. M. Heijmans and C. Ronse, "The Algebraic Basis of Mathematical Morphology I. Dilations and Erosions," *Computer Vision, Graphics, and Image Processing*, vol. 50, no. 3, pp. 245-295, June 1990.
- [25] J. Serra, "Introduction to Mathematical Morphology," *Computer Vision, Graphics, and Image Processing*, vol. 35, pp. 283-305, 1986.
- [26] F. Meyer, "Automatic Screening of Cytological Specimens," *Computer Vision, Graphics, and Image Processing*, vol. 35, pp. 356-369, 1986.

- [27] R. M. Haralick, S. R. Sternberg, and X. Zhuang, "Image Analysis using Mathematical Morphology," *IEEE Transactions on Pattern Analysis and Machine Intelligence*, vol. PAMI-9, no. 4, pp. 532-550, July 1987.
- [28] S. R. Sternberg, "Greyscale Morphology," *Computer Vision, Graphics, and Image Processing*, vol. 35, pp. 333-355, 1986.
- [29] R. M. Loughheed, D. L. McCubbrey, and S. R. Sternberg, "Cytocomputers: Architectures for Parallel Image Processing," in *Proceedings of the Workshop on Picture Data Description and Management*, Pacific Grove, CAL, Aug. 27-28, 1980, pp. 282-286.
- [30] X. Zhuang and R. M. Haralick, "Morphological Structuring Element Decomposition," *Computer Vision, Graphics, and Image Processing*, vol. 35, pp. 370-382, 1986.
- [31] I. Pitas and A. N. Venetsanopoulos, "Morphological Shape Decomposition," *IEEE Transactions on Pattern Analysis and Machine Intelligence*, vol. PAMI-12, no. 1, pp. 38-45, Jan. 1990.



## Vita Auctoris



John Cardillo was born in Windsor, Ont., Canada on November 7, 1963. He received his B.A.Sc. degree in 1986 and his M.A.Sc. degree in 1988, both in Electrical Engineering from the University of Windsor, Windsor, Ont., Canada. Currently he is a candidate for the doctoral degree in Electrical Engineering at the University of Windsor and is expected to graduate in June 1991. His research interests include machine vision, image processing, and robotics. His Ph.D.

research is in the field of biomedical image processing.